

# **UC San Diego**

## **UC San Diego Previously Published Works**

### **Title**

Reduced evolutionary constraint accompanies ongoing radiation in deep-sea anglerfishes

### **Permalink**

<https://escholarship.org/uc/item/9nf2z32d>

### **Journal**

Nature Ecology & Evolution, 9(3)

### **ISSN**

2397-334X

### **Authors**

Miller, Elizabeth Christina

Faucher, Rose

Hart, Pamela B

et al.

### **Publication Date**

2025-03-01

### **DOI**

10.1038/s41559-024-02586-3

### **Copyright Information**

This work is made available under the terms of a Creative Commons Attribution License, available at <https://creativecommons.org/licenses/by/4.0/>

Peer reviewed

# Reduced evolutionary constraint accompanies ongoing radiation in deep-sea anglerfishes

Received: 3 November 2023

Accepted: 18 October 2024



Check for updates

Elizabeth Christina Miller <sup>1,2,3,4,5,11</sup>, Rose Faucher<sup>6,11</sup>, Pamela B. Hart<sup>1,2,7</sup>, Melissa Rincón-Sandoval <sup>1</sup>, Aintzane Santaquiteria <sup>1</sup>, William T. White <sup>8</sup>, Carole C. Baldwin <sup>9</sup>, Masaki Miya<sup>10</sup>, Ricardo Betancur-R <sup>1,2,5</sup>, Luke Tornabene<sup>3,4</sup>, Kory Evans<sup>6</sup> & Dahiana Arcila <sup>1,2,5</sup>

Colonization of a novel habitat is often followed by phenotypic diversification in the wake of ecological opportunity. However, some habitats should be inherently more constraining than others if the challenges of that environment offer few evolutionary solutions. We examined this push-and-pull on macroevolutionary diversification following habitat transitions in the anglerfishes (Lophiiformes). We constructed a phylogeny with extensive sampling (1,092 loci and ~38% of species), combined with three-dimensional phenotypic data from museum specimens. We used these datasets to examine the tempo and mode of phenotypic diversification. The deep-sea pelagic anglerfishes originated from a benthic ancestor and shortly after experienced rapid lineage diversification rates. This transition incurred shifts towards larger jaws, smaller eyes and a more laterally compressed body plan. Despite these directional trends, this lineage still evolved high phenotypic disparity in body, skull and jaw shapes. In particular, bathypelagic anglerfishes show high variability in body elongation, while benthic anglerfishes are constrained around optimal shapes. Within this radiation, phenotypic evolution was concentrated among recently diverged lineages, notably those that deviated from the archetypical globose body plan. Taken together, these results demonstrate that spectacular evolutionary radiations can unfold even within environments with few ecological resources and demanding physiological challenges.

How do lineages evolve after colonizing new environments? Ecological opportunity in a novel habitat can become the kindling for evolutionary radiation<sup>1–4</sup>. However, if environmental conditions of the new habitat present different challenges from the ancestral habitat, the lineage could experience strong selection towards adaptive optima that allow it to overcome these challenges. While evolution can be rapid in this scenario, if there are few evolutionary solutions to an environmental problem, then phenotypic diversity should be low<sup>5</sup>. If some

environments are inherently more constraining than others, then this push-and-pull of radiation versus adaptation may explain why diversity varies across habitats<sup>6</sup>.

The bathypelagic zone of the deep sea (>1,000 m) is characterized by a lack of solar light, limited food, high pressure, low temperatures and large expanses of homogeneous space<sup>7–10</sup>. Deep pelagic fishes converged on specializations including large jaws and teeth, sedentary behaviour, reduced musculature and skeletal architecture, small but

sensitive eyes and bioluminescence<sup>7,8,11–19</sup>. The repeated evolution of these adaptations across distantly related lineages is an indication that there are a limited number of solutions to overcome the challenges of the bathypelagic zone<sup>20</sup>.

Compared with the deep sea and open ocean, coastal marine environments such as coral reefs and estuaries are productive and topologically complex<sup>21,22</sup>. Due to their more pronounced biotic and abiotic clines, and presumably greater number of niches, we should expect coastal ecosystems to promote ecological, morphological and lineage diversification relative to other marine settings. This expectation is well substantiated by numerous empirical studies across diverse taxa<sup>23–30</sup>. Yet, recent studies using phylogenetic comparative methods have shown that fishes from less-productive oceanic habitats can still have high phenotypic disparity and diversification rates<sup>31–35</sup>, contradicting expectations based on ecological principles<sup>36</sup>. The nature of such diversification in deep-sea organisms is still poorly understood. For example, it is unclear whether high evolutionary rates are characteristic of all deep-sea habitats. The ‘deep sea’ (marine environments >200 metres) circumscribes a collection of habitats with variable selective pressures<sup>7</sup> and different evolutionary histories of the lineages in each habitat<sup>7,14,15,37</sup>.

The anglerfishes (order Lophiiformes) are an iconic clade of marine fishes whose members are characterized by a lure on their head that is used for sit-and-wait hunting. Lophiiformes contains ~350 species among five well-supported suborders: Lophioidei (monkfishes), Ogocephaloidei (batfishes), Antennarioidei (frogfishes), Chaunacoidei (sea toads) and Ceratioidei (dreamers and sea devils)<sup>38</sup>. Four of the five suborders are benthic (resting on the seafloor) in shallow and deep-sea settings, while the ceratioids are deep pelagic (live within the water column >300 m and most commonly >1,000 m)<sup>12</sup>. The ceratioids are known for their extreme sexual size dimorphism and varying degrees of sexual parasitism in which males fuse to a female, a phenomenon not found in any other vertebrate<sup>39,40</sup>. In addition to their habitat diversity, anglerfishes also exhibit diverse body shapes ranging from laterally compressed, dorsoventrally compressed, globose and elongate. While the pelagic ceratioids are known among scientists and non-scientists alike for their bizarre adaptations, their benthic relatives are also atypical fishes. Specializations of benthic anglerfishes include extreme oral gape expansion<sup>41</sup>, a tetrapod-like walking gait<sup>42</sup> and extremely slow breathing in low-oxygen settings<sup>43,44</sup>. It is believed that their unusual shapes are related to the evolution of restricted gill openings, which frees constraints on cranial morphology<sup>45</sup> and allows the body to fill with water to perform these specialized functions.

How have habitat transitions shaped the diversity of anglerfishes? One hypothesis is that shallow-water and/or deep benthic lineages will have faster rates of phenotypic and lineage diversification than the bathypelagic ceratioids. Deep benthic environments are generally more heterogeneous than deep pelagic counterparts<sup>9,37,46</sup>. For example, there is evidence from remotely operated vehicle (ROV) videos that closely related benthic anglerfish species have different substrate preferences<sup>47–49</sup>. In contrast, the environmental homogeneity of the open ocean below 1,000 m is unparalleled on Earth<sup>8</sup>. There are few barriers to dispersal, which should limit speciation in principle<sup>50–52</sup> (but see refs. 53–56). Further, the environmental challenges that characterize the bathypelagic zone over other deep-sea habitats<sup>7,14</sup> should impose constraints on evolution, limiting the number of viable phenotypes<sup>20</sup> and thereby reducing rates of phenotypic evolution<sup>5</sup>.

An alternative hypothesis is that the bathypelagic anglerfishes have faster rates of diversification and are less evolutionarily constrained than shallow-water or deep benthic relatives. Due to the lack of solar light, predator–prey interactions occur over shorter spatial scales in the deep sea than in shallow waters, often facilitated by lurking and bioluminescence<sup>8,15,57</sup>. This presumably reduces selection for

the fusiform body shapes common among shallow-water pelagic predators<sup>28,29,32,35,58–61</sup>, allowing bathypelagic anglerfishes to explore new areas of morphospace. If this hypothesis is supported, we would expect ceratioid morphological disparity to be higher than that of benthic relatives. In addition, if this ecological release is associated with faster rates of lineage and phenotypic diversification and the filling of novel ecological niches<sup>3,62</sup>, then ceratioids could be a rare example of a deep-sea adaptive radiation<sup>1,63</sup>. This would be noteworthy because most adaptive radiations are known from environments with abundant ecological resources<sup>1</sup>. Even the concept of adaptive radiation itself seems at odds with the bathypelagic zone for its apparent dearth of niches<sup>64</sup>.

Dense species sampling is needed to gain power for phylogenetic comparative methods<sup>65</sup>. However, progress in building phylogenies of deep-sea fishes has been slowed by the difficulty of collecting specimens<sup>9,66,67</sup>. Here we present a phylogenomic hypothesis of anglerfishes based on 1,092 single-copy exon markers. Due to contributions from many natural history collections and government agencies<sup>68,69</sup>, our taxonomic sampling improves upon that of all predecessors<sup>40,70–72</sup>, with nearly 40% of species and all deep-sea families sampled. This advance allowed us to apply phylogenetic comparative methods largely reserved for well-sampled terrestrial and shallow-water organisms to test hypotheses about macroevolution in the deep sea.

## Results

### Phylogenomic inference and divergence times

We generated genomic data for 152 lophiiform individuals from 120 species using exon capture approaches proven successful for fishes<sup>61,73–75</sup> (Supplementary Table 1). Sampling was augmented by mining exons from published ultra-conserved elements (UCEs)<sup>71,72</sup> and legacy markers from the National Center for Biotechnology Information (NCBI) (Supplementary Tables 2 and 3). Final taxonomic sampling after quality control included 132 species of Lophiiformes (37.8% of species) and 20 of 21 families (all but Lophichthyidae). Sampling of the bathypelagic ceratioids included all 11 families and 32.1% of species. The taxonomic sampling of this tree is comparable to many other fish clades. For comparison, the largest published phylogeny of ray-finned fishes sampled ~11,000 species or roughly 37% of described actinopterygians<sup>76</sup>. Other recent anglerfish phylogenies sampled 14–27% of Lophiiformes and 9–21% of ceratioids<sup>40,71</sup>.

Systematic relationships were largely in agreement between concatenation- and coalescent-based phylogenomic analyses (Supplementary Appendix 1 in ref. 77). Detailed systematic results are given in Supplementary Appendix 2. We assembled a set of 21 node calibrations, including eight outgroup and ten ingroup fossils and three geologic calibrations (Supplementary Appendix 3). We aimed to be comprehensive with our calibration scheme, including all relevant lophiiform fossils from the Eocene Monte Bolca communities<sup>78</sup> (Fig. 1). To incorporate uncertainty in topology and divergence times for comparative analyses, we produced eight alternative time trees using either the IQ-TREE or ASTRAL tree, a calibration scheme with or without the controversial fossil †*Plectocretacicus*<sup>75,79</sup> and using either MCMCTree<sup>80,81</sup> or RelTime<sup>82,83</sup> as the calibration method.

Six out of eight time trees inferred a Cretaceous origin of crown Lophiiformes (92–61 Ma across trees) (Fig. 1). The methodological choice with the largest impact on divergence times was the use of MCMCTree versus RelTime. In the MCMCTrees, Ceratioidei diverged from Chauancoidei near the Cretaceous–Paleogene (K–Pg) boundary (67 million years ago (Ma)), whereas in the RelTime trees this divergence occurred in the Eocene (47–40 Ma). Similarly, the two methods resulted in a >20 million-year difference in the crown age of Ceratioidei, either in the Palaeocene (~58 Ma using MCMCTree) or late Eocene (40–34 Ma using RelTime). This variation makes it difficult to attribute this singular benthic-to-bathypelagic transition with any geologic event<sup>40</sup>. Detailed comparison of divergence times with previous

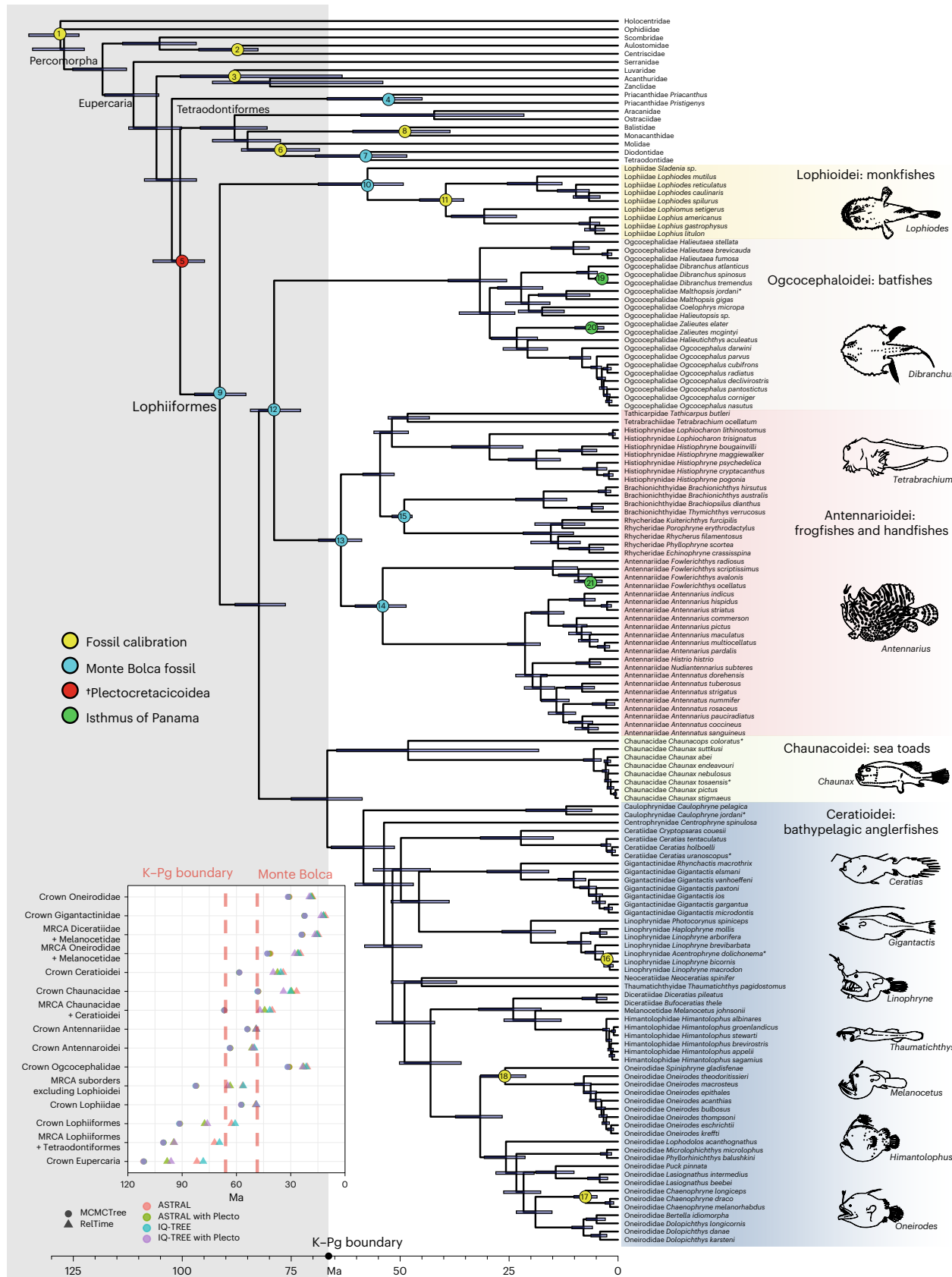


**Fig. 1 | A time-calibrated phylogeny of Lophiiformes based on exon capture.** Tip labels in bold were added by mining exons from published UCE alignments. Asterisks indicate tip labels in bold were added using legacy markers. Tree shown was inferred using IQ-TREE and calibrated using MCMCTree with the scheme including +Plectocretacoidea. (for the RelTime equivalent,

see Supplementary Appendix 1 in ref. 77). Calibrations are numbered as in Supplementary Appendix 3. Inset: the range of dates for key nodes inferred across the eight alternative time trees (with and without +Plectocretacoidea). Line art reproduced with permission from ref. 190 Food and Agriculture Organization of the United Nations.

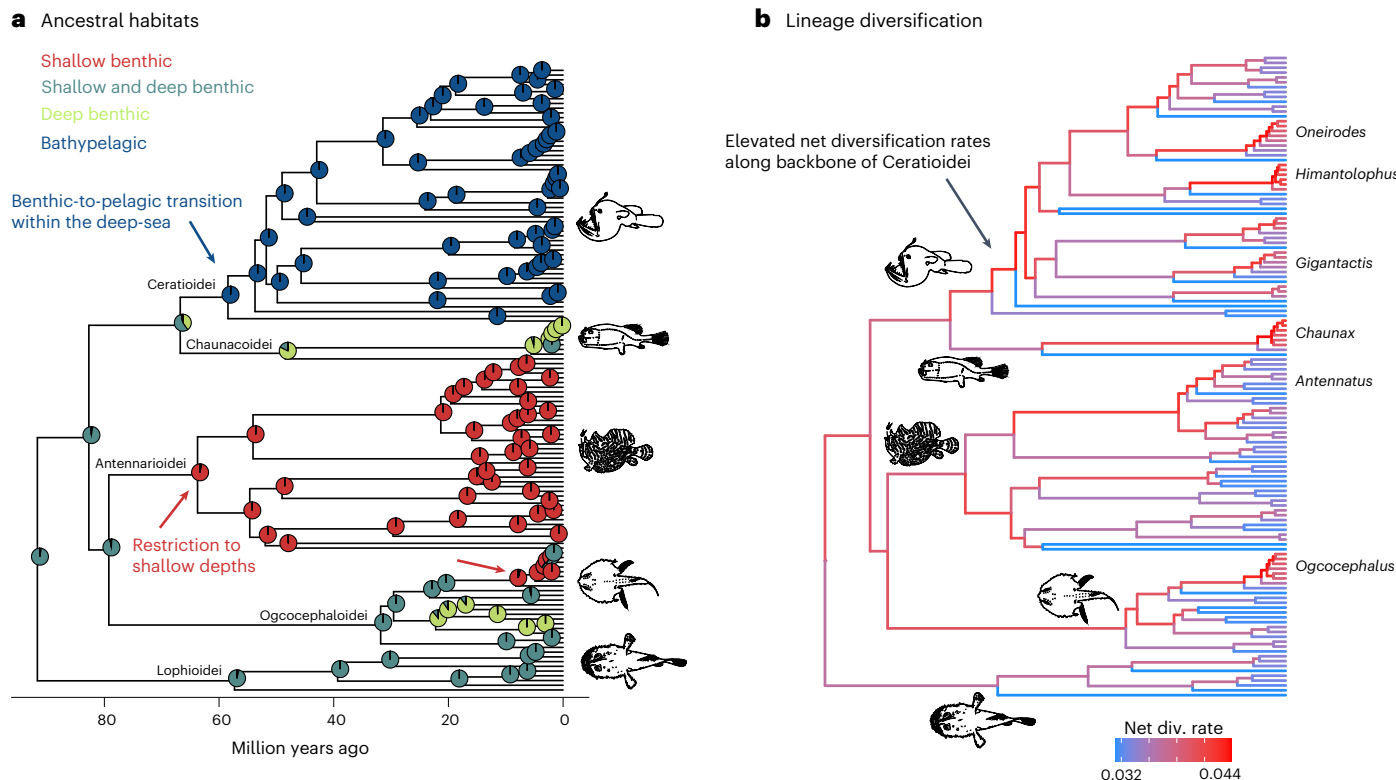


**Fig. 2 | Habitat transitions and lineage diversification rates.** **a,b**, IQ-TREE calibrated using MCMCTree without †Plectocretacicoidea. **a**, Habitat reconstructions inferred using BioGeoBEARS. To compare results based on

all trees, see Extended Data Fig. 1. **b**, Model-averaged net diversification (div.) rates inferred using MiSSE. For tip-associated rates across all trees, see Extended Data Fig. 2.

studies, including justification for our older age estimates, is given in Supplementary Appendix 4.

### Habitat transitions

Ancestral habitat reconstructions (Supplementary Table 4) based on the best-fitting biogeographic model (BAYAREA + J in all cases; Supplementary Table 5) indicated that the ancestor of all Lophiiformes had a widespread depth range spanning the continental shelf and slope<sup>84</sup> (Fig. 2a). The bathypelagic ceratioids originated from a benthic continental slope ancestor. In other words, the most relevant habitat transition associated with the ceratioid radiation was benthic-to-pelagic, not shallow-to-deep. There were two transitions to a shallow-only habitat within Lophiiformes: at the origin of frogfishes (Antennarioidei) and the batfish genus *Ogocephalus*. Ancestral states were nearly identical across all input trees (Extended Data Fig. 1).

### Lineage diversification rates

We estimated branch-specific net diversification rates using the missing state speciation and extinction (MiSSE) framework<sup>85</sup>. MiSSE models with 1–7 rate classes were supported with >5% of the relative Akaike weight across alternative trees (Supplementary Table 6). There was little consensus on a best-fit model for any tree, therefore we model-averaged the rates<sup>86</sup>. The backbone of Ceratioidei following the benthic-to-pelagic transition had high net diversification rates (Fig. 2b). The distributions of more recent (tip-associated) rates of net diversification overlapped among habitats (Extended Data Fig. 2), suggesting no enduring tendency for lineage diversification rates to vary by habitat. Pruning for suspected taxonomic inflation in certain genera (Supplementary Appendix 2) reduced rate variation overall, but the general patterns remained (Extended Data Fig. 2).

### Phenotypic diversity of anglerfishes

The five lophiiform lineages segregated in morphospace according to clade-specific body plans (Fig. 3a). The first principal component (PC) axis of the body shape morphospace was associated with lateral versus dorsoventral compression of the body and small versus large eyes. The second PC axis corresponded to variation in body elongation and mouth size, with compact bodies and small mouths having low values, and elongate bodies and large mouths having high values. Based on the position of the ceratioids in morphospace, the transition from deep benthic to deep pelagic habitats incurred an increase in jaw size, decrease in eye size and lateral compression of the body. Continental shelf taxa generally had shorter bodies and smaller mouths compared with deep-sea relatives. The morphospace of body shape was comparable whether linear measurements were size-corrected using log-shape ratios versus phylogenetic generalized least squares (PGLS) residuals, the latter of which removes the effect of allometry (Extended Data Fig. 3).

In addition to body shape, we quantified cranial shape on the basis of geometric morphometrics using micro-computed tomography ( $\mu$ CT) scans (Extended Data Fig. 4 and Supplementary Table 7). Most ceratioids had similar skull shapes as deep-benthic relatives, although some taxa explored novel regions of morphospace (Fig. 3b). The first PC axis was related to variation in elongation of the skull and the size and position of the jaws and orbit (with the batfish *Ogocephalus* having the lowest values and the wolffish angler *Thaumaticichthys* having the highest values). Continental shelf taxa were restricted to an area of morphospace associated with shorter and narrower skulls with the orbits positioned high on the head. The second PC axis was related to size and compression of the neurocranium, generally describing a batfish-like skull on the positive end and a frogfish-like skull on the negative end.

The bathypelagic ceratioids deviated strongly from deep-benthic relatives in jaw shape, whereas they did not for overall cranial shape

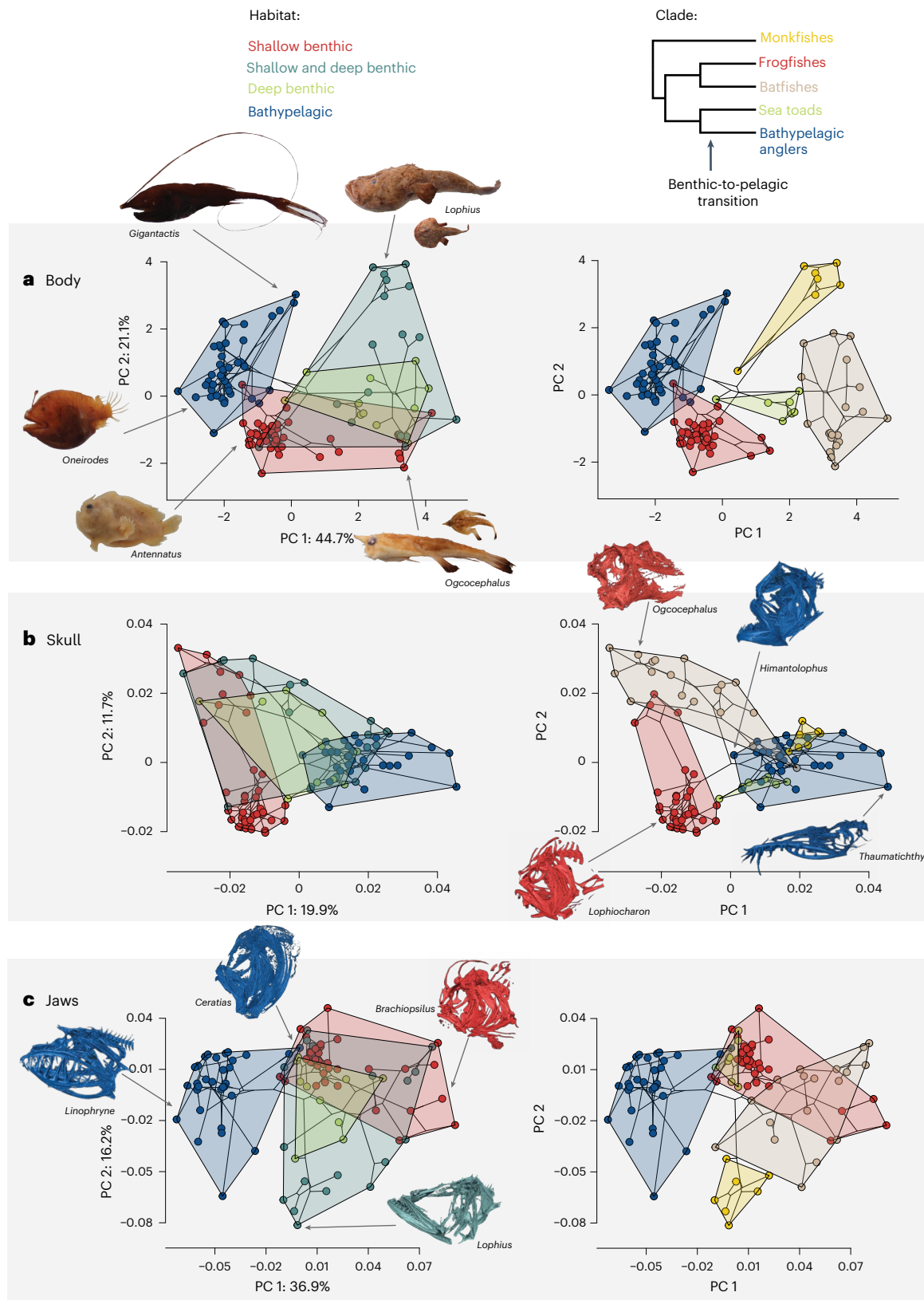


**Fig. 3 | Phenotypic diversity of anglerfishes.** Phylogenomorphospace visualizations of (a) body shape, (b) skull shape and (c) jaw shape. Left: polygons grouping taxa by habitat. Right: polygons grouping taxa by suborder. For comparison of body shape morphospaces with different size-correction strategies, see Extended Data Fig. 3.

(Fig. 3c). The first PC axis of jaw morphospace described the length of the jaws, from short and robust on the positive end (frogfishes and batfishes) to long and thin on the negative end (most ceratioids). The second PC axis corresponded to variation in lateral versus dorsoventral

compression of the jaws (for example, frogfishes versus monkfishes). Departing from the overall trend, one bathypelagic family (Ceratiidae) secondarily evolved a jaw shape more similar to shallow-water frogfishes than to other ceratioids (Fig. 3c).

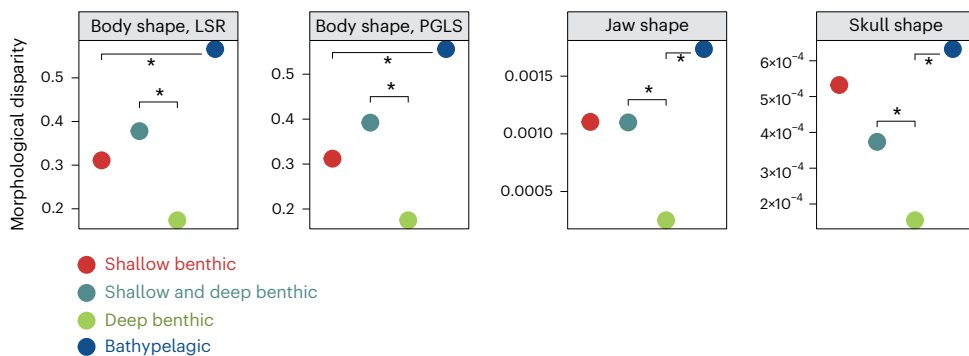


**Fig. 4 | Phenotypic disparity by habitat.** Asterisks indicate significant pairwise comparisons. LSR, size corrected using log-shape ratios. PGLS, size corrected using PGLS residuals that remove the effects of allometry. For full disparity results, see Supplementary Appendix 5 in ref. 77 and Extended Data Fig. 9.

Despite the directional evolutionary trends described above, bathypelagic ceratioids contained the highest shape disparity<sup>87</sup>, while deep-sea benthic taxa contained the least disparity (Fig. 4). Shallow-water taxa contained intermediate levels of disparity, as did taxa spanning the continental shelf and slope. These patterns were consistent across all four multivariate datasets (body shape based on two alternative size-correction strategies, skull shape and jaw shape). Since the sister group to the ceratioids is deep benthic (sea toads), these results support the hypothesis that this benthic-to-pelagic transition promoted phenotypic diversification.

### Temporal shifts in phenotypic diversification

We took advantage of flexible analytical approaches for modelling the evolution of complex phenotypes<sup>88–90</sup>. The best-fitting model of phenotypic evolution was generally a variable-rates Ornstein–Uhlenbeck (OU) model with separate optima for each habitat, although an early-burst model received similar support in some cases (Extended Data Fig. 5). This is unsurprising since both models reflect components of Simpson’s model of diversification<sup>91,92</sup>. The output of variable-rate BayesTraits analyses<sup>88,93</sup> is a posterior distribution of trees in which the branches are scaled proportional to the degree of morphological change<sup>93</sup>, allowing us to visualize evolutionary shifts across anglerfishes (Fig. 5 and Extended Data Fig. 6). Under the multi-optima OU model, branch-length scalars reflect the evolutionary rate as well as the strength of selection towards each habitat’s optimal shape. Since these factors cannot be separated (making interpretation difficult), we also visualized results on the basis of a Brownian motion model in which branch-length modifications can be directly interpreted as rate variation<sup>88,93</sup> (Extended Data Fig. 6).

Three trends in anglerfish diversification were consistent from BayesTraits analyses based on different underlying models, phenotypic datasets, input trees and treatment of allometry (Fig. 5 and Extended Data Fig. 6). First, branches associated with divergence among suborders were often associated with a high degree of morphological change, especially in body shape. This implies that phenotypic variation was partitioned early in the history of Lophiiformes, consistent with our morphospace visualization (Fig. 3). Second, continental shelf taxa, especially frogfishes, tended to show limited phenotypic change, seemingly due to low rates of evolution (Extended Data Fig. 6). Third, within the ceratioid radiation, morphological evolution was concentrated among recently diverged lineages, suggesting that phenotypic diversification has been generally offset from lineage diversification (Fig. 2b). Elevated phenotypic change was particularly associated with taxa that deviated from the canonical ‘globose’ body shape of popular imagination, as illustrated by the wolffang angler *Lasiognathus* and *Thaumaticthys* and the whipnose angler *Gigantactis* (Figs. 5 and 6). The leftvent anglers *Haplophryne* and *Linophryne* were innovators in cranial and jaw shape (Fig. 5). Altogether, these results suggest the order Lophiiformes is characterized by a complex history that

combines an early burst of body shapes with more recent specialization and innovation, especially within the ceratioids.

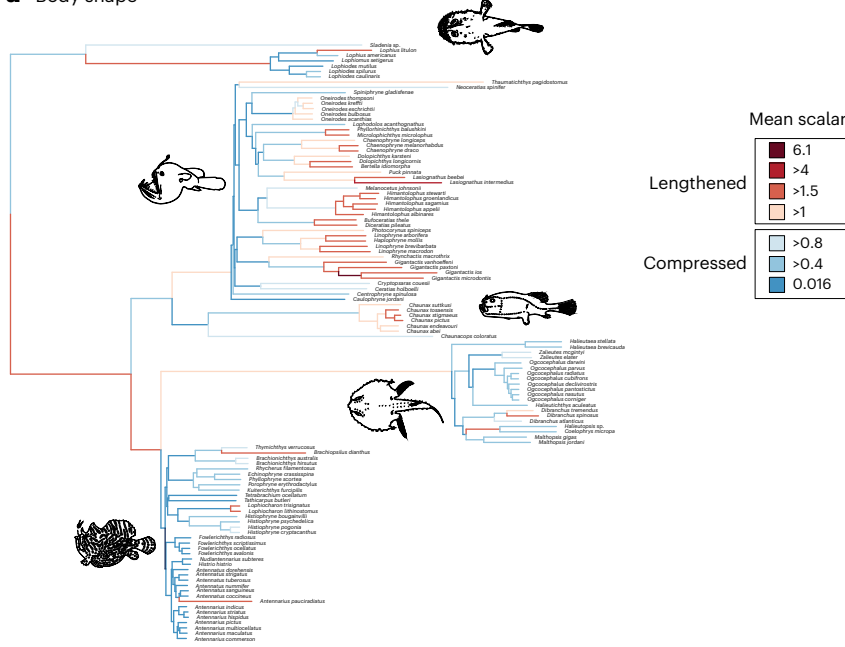
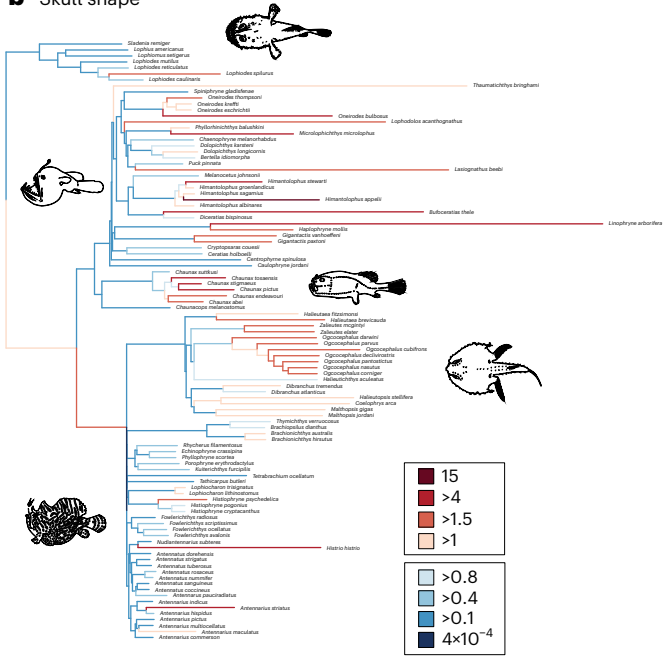
### Evolution along individual shape dimensions

Habitats impose selection on some aspects of phenotype more strongly than others. To evaluate the differential effects of selection, we fit univariate evolutionary models on ten body shape traits individually (Extended Data Fig. 7). In all cases, an OU model with variable optima for each habitat was preferred over Brownian motion or single-optima OU models (Supplementary Table 8). Compared with deep benthic lophiiforms, ceratioids showed evolutionary optima towards longer jaws, smaller eyes, larger interorbital distances (more spacing between the eyes) and deeper bodies, suggesting directional selection (Extended Data Fig. 7). Traits that seemed to be under less constraint in ceratioids than benthic taxa, as inferred from their wider variation, included standard length and caudal peduncle depth and width (reflecting the robustness of the tail, which is used to generate thrust in most fishes). Although they all have generally small eyes, ceratioids surprisingly show wide variation in eye diameter relative to their body size (Extended Data Fig. 7). In addition to higher variation, these traits had higher evolutionary rates in ceratioids compared with deep-benthic lophiiforms (Extended Data Fig. 8). These patterns were corroborated by univariate analyses of disparity (Extended Data Fig. 9 and Supplementary Appendix 5 in ref. 77).

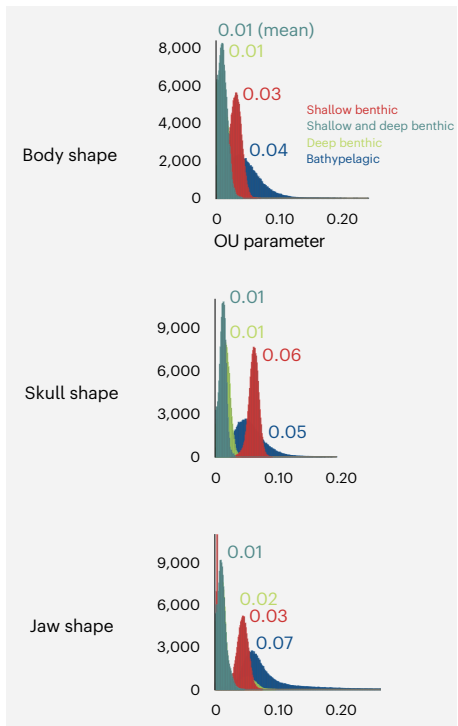
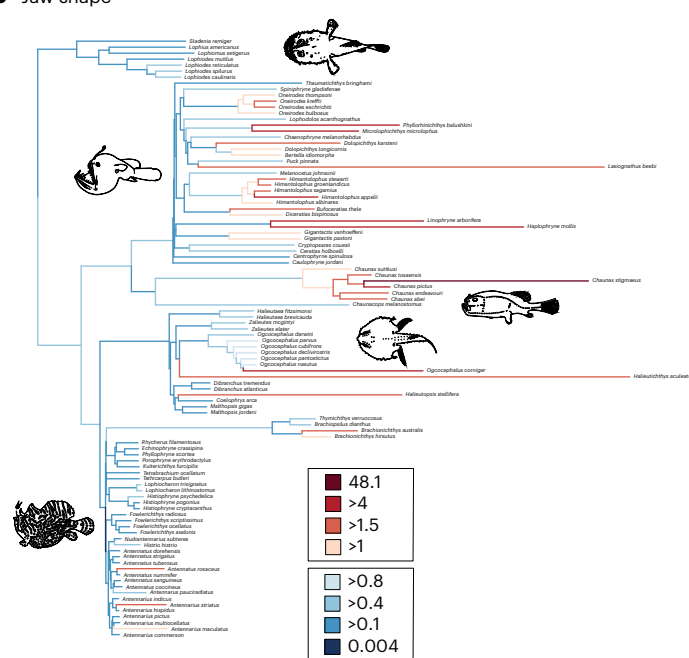
Of all traits, evolutionary trends in standard length are especially noteworthy: ceratioids show greater disparity and faster rates of evolution of standard length than benthic lophiiforms (Fig. 6), regardless of the means of size correction or input tree (Extended Data Figs. 7–9 and Supplementary Appendix 5 in ref. 77). Since standard length reflects body elongation when size corrected with log-shape ratios<sup>94</sup>, this result indicates that elongation is under less constraint than other shape dimensions of ceratioids. It also indicates that elongation is less constrained in the ceratioids compared with benthic anglerfishes. In addition, standard length measurements do not show signs of bias associated with preservation artefacts of delicate specimens (Extended Data Fig. 10).

### Discussion

Here we asked whether colonization of a novel but challenging environment should promote or constrain macroevolutionary diversification. Colonization of new environments is widely believed to be a precursor to taxonomic and phenotypic diversification<sup>4</sup>. Yet, some environments should be inherently more constraining than others, potentially because there are few available niches or the challenges of that habitat only have a few viable solutions<sup>5,6,20</sup>. Using a suite of phylogenetic comparative methods, we found that the bathypelagic ceratioids originated from a deep-sea benthic ancestor and subsequently experienced rapid lineage diversification. Phenotypic novelty evolved repeatedly within this radiation, despite directional selection on morphologies related to adaptation to the dark and resource-poor bathypelagic environment.

**a Body shape****b Skull shape**

**Fig. 5 | Morphological change through time.** BayesTraits results of (a) body shape, (b) skull shape and (c) jaw shape are shown on the basis of an OU model with local optima associated with habitat. Branch lengths are scaled according to morphological change, reflecting the OU parameter (strength of selection; shown in grey panel) and evolutionary rate. Warm colours and scalars >1 indicate

**c Jaw shape**

that the branch length was increased; cool colours and scalars <1 indicate that the branch length was compressed. For results under a Brownian motion model (in which scalars are directly interpretable as rate variation) and comparing input trees and effects of allometry, see Extended Data Figs. 5 and 6.

Taken together, these results demonstrate that environmental constraints do not always inhibit macroevolutionary diversification. The bathypelagic zone imposes constraints on some aspects of phenotype but releases constraints on other aspects, allowing evolutionary radiation to unfold even in resource-poor settings.

### Diversification of benthic anglerfishes

The order Lophiiformes contains many of the most atypically shaped fishes<sup>94</sup>, including the invertebrate-mimicking frogfishes<sup>41</sup>, the flattened

batfishes and monkfishes, and the globose sea toads and ceratioids. The five suborders of Lophiiformes occupy distinct regions of the body shape morphospace (Fig. 3a), and the appearance of these characteristic body plans was associated with high evolutionary rates (Fig. 5). These results fit the predictions of Simpson's conceptualization of macroevolutionary diversification<sup>91,92</sup>, in which lineages occupy 'adaptive zones' that canalize future diversification. The early appearance of lophiiform body plans is also preserved in the fossil record: Eocene fossils resemble living monkfishes, frogfishes and batfishes<sup>95–100</sup>.

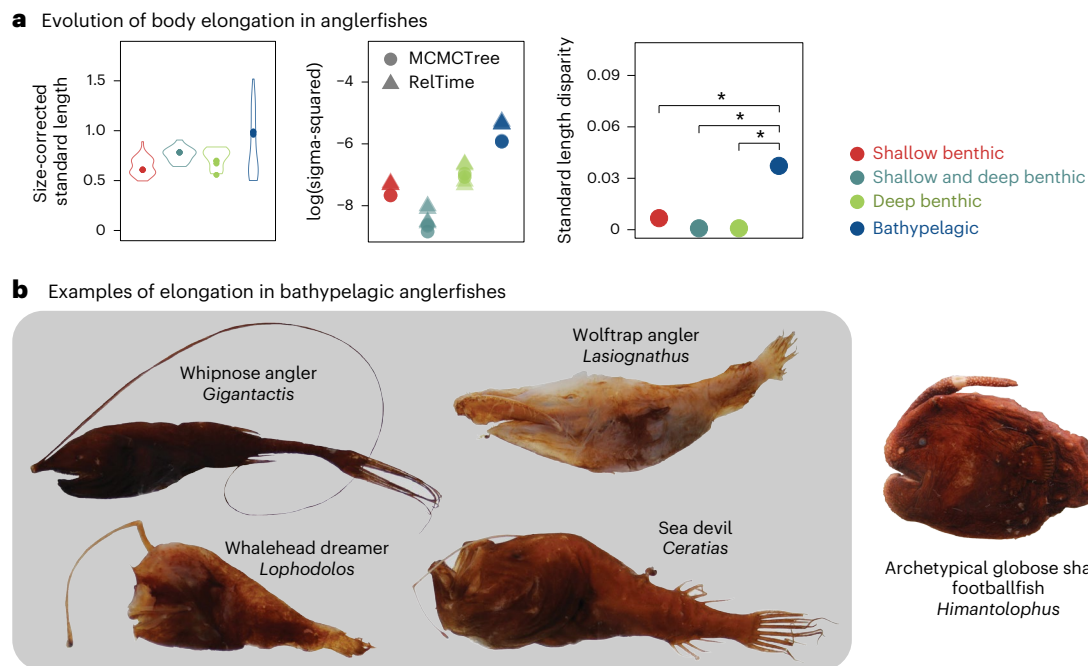


**Fig. 6 | Evolution of body elongation across anglerfishes.** **a**, OUwie results and variation in standard length. Left: variation in standard length (size corrected using log-shape ratios) with OU optimum for each habitat marked with a circle for each input tree. Middle: rate of standard length evolution under a multiple-peak

OU model, inferred using eight input trees. Right: disparity in standard length by habitat. Asterisk indicates significant pairwise comparisons. **b**, Photographs depicting examples of elongated ceratioids compared with a globose relative.

Studies of other marine organisms suggest that coastal shelf habitats, especially coral reefs, promote phenotypic evolution<sup>23,25,26,29,101</sup>. Yet, the most reef-associated clade of anglerfishes, the frogfishes, was relatively constrained in body and skull shape, fitting a pattern of ‘branch packing’<sup>90</sup> (Fig. 3). Frogfishes had the lowest rates of multivariate phenotypic evolution among anglerfishes (Fig. 5 and Extended Data Fig. 6). The other anglerfish clade that specialized on continental shelf habitats, the batfish genus *Ogcocephalus*, was likewise restricted in morphospace relative to deep-sea batfishes (Fig. 3). Therefore, anglerfishes reverse the well-documented phenomenon seen in other taxa for coastal habitats to be a diversity pump<sup>23–25,101–103</sup>.

Why are frogfishes so morphologically similar to each other despite occupying variable and complex coastal habitats? Unlike other reef fish clades<sup>25,104</sup>, frogfishes neither evolved novel diets nor partitioned dietary resources more finely on reefs compared with relatives in other habitats. They are indiscriminate carnivores with extensible stomachs capable of the largest volume of oral expansion known among reef fishes, allowing them to catch prey from long distances using suction feeding<sup>41</sup>. Evolutionary innovations may result in specialization instead of diversification if the innovation does not broaden the array of potential resources<sup>105,106</sup>. We might therefore conclude that the frogfish bauplan functions in a variety of coastal environments by increasing their success as a generalist carnivore, and there is little selective incentive to modify it even with the genetic and developmental ability to do so<sup>30,107,108</sup>.

### Evolutionary radiation in the bathypelagic zone

The bathypelagic ceratioids occupied a region of morphospace associated with small eyes, large jaws and laterally compressed, sometimes elongate bodies (Fig. 3). This suggests that these features are a response to bathypelagic conditions versus benthic habitats of similar depth<sup>7,14</sup>. Still, we found that ceratioids had higher phenotypic disparity than anglerfishes restricted to shallow or deep-sea benthic habitats (Figs. 4 and 6). Ceratioid diversification includes instances of convergence on shallow-water shapes (Fig. 3c), as well as the evolution of

novel phenotypes related to hunting. Most strikingly, the ‘wolftrap’ phenotype<sup>12</sup>, in which the body is elongate and the upper jaw hangs above the lower jaw, evolved twice (in *Lasiognathus* and *Thaumatichthys*) and is seemingly associated with high rates of evolution (Fig. 5 and Extended Data Fig. 6). Ceratioids especially show substantial diversity on the spectrum of body elongation (Fig. 6). Even though the public is most familiar with an ‘archetypical’ globose anglerfish shape, elongate forms are also common including *Ceratias*, *Gigantactis* and the wolftrap anglers. Ceratioids have therefore been able to diversify as long as loose constraints related to a bathypelagic existence are satisfied.

Are the bathypelagic ceratioids an adaptive radiation<sup>1,2</sup>, or can their diversity be explained by non-adaptive processes<sup>109–111</sup>? This is not a pedantic exercise<sup>109</sup> but is crucial for understanding fundamental questions about deep-sea evolution. For example, given the paucity of resources, is adaptive radiation even possible in the deep sea? If so, does it conform to patterns described for terrestrial, freshwater and shallow marine adaptive radiations<sup>1</sup>? A shared element among all definitions of adaptive radiation is that lineages diverge in phenotype as they capitalize on different ecological resources<sup>63</sup>. We know very little about what ecological opportunity looks like in the deep sea. On one hand, bathypelagic habitats are among the most food-limited and environmentally homogeneous settings on Earth. On the other hand, population density of bathypelagic fishes is low and populations are spread across the globe<sup>12,52</sup>. Environments with patchy resources should promote coexistence by preventing any species from becoming dominant<sup>112</sup>. Therefore, resources are limited, but competitive pressure should be diffuse<sup>113</sup>.

Ecological opportunity, the kindling that fuels adaptive radiation, is thought to be highest upon colonizing a novel habitat that lacks competitors, especially when coupled with a key innovation that provides access to novel resources<sup>1,3,4</sup>. Ceratioids are by far the most diverse vertebrate clade in the bathypelagic zone today<sup>12</sup>. Their lure, large jaws, low metabolism and extensible stomachs are shared with their benthic relatives<sup>41,44</sup>, traits which may have predisposed them for success in the food-limited deep sea relative to non-lophiiiform competitors<sup>11,56</sup>. The

base of the clade showed high lineage diversification rates coincident with the benthic-to-pelagic transition (Fig. 2). Their sister group, the deep-benthic sea toads, have comparably low taxonomic and phenotypic diversity<sup>111</sup> (Fig. 3). These pieces of evidence fit the search image of an adaptive radiation<sup>2</sup>.

What more is needed to be confident in the nature of the ceratioid radiation? Some authors believe that without clear linkages between phenotypic, functional and ecological diversity, a non-adaptive radiation is the appropriate null expectation<sup>2</sup>. Although there is evidence for a relationship between form and function in ceratioids<sup>114</sup>, the relationship between function and ecology remains anecdotal. For example, our geometric morphometric analyses (Fig. 3c) support a recent study based on linear morphometrics that ceratioids have diverse jaw shapes<sup>114</sup>. This study also demonstrated that diversity in form yielded differences in function, such that ceratioids differ in the speed and force with which they close their jaws<sup>114</sup>. Despite high variation in shape and function of feeding morphologies, ceratioids seem to be dietary generalists<sup>15,115</sup>. We know from videos and trawl records that some taxa visit the benthic boundary layer, with demersal prey making up some portion of their diet<sup>12,37,114,116,117</sup>. Otherwise, evidence of phenotype–ecology matching is sorely lacking.

The alternative explanation, that phenotypic and functional diversity are unrelated to ecological diversity, has not yet been falsified for this group. One possibility is that phenotypic diversity arose from random mutations that were not removed by selection and thereby maintained over macroevolutionary timescales<sup>118</sup>. Bathypelagic fishes have neither the demands of shallow-water pelagic predators for pursuing prey<sup>58</sup> nor the challenges of navigating obstacles as for benthic fishes<sup>28,32</sup>. Such relaxed selection due to ecological release is believed to play an important role in the initial stages of adaptive radiation by broadening phenotypic diversity, giving way to a later stage of disruptive selection among these phenotypes<sup>13,62,118</sup>. However, it is unclear what would prompt this initial phase of relaxed selection to give way to disruptive selection<sup>119</sup> in the bathypelagic zone, considered to be among the most environmentally stable habitats on Earth<sup>113</sup>. Ceratioid body elongation may fit this evolutionary pattern (Fig. 6). In-life videos suggest that globular<sup>120</sup> and elongate<sup>116</sup> ceratioids are both incapable of sustained swimming due to their reduced skeletons and musculature. While elongation is a common theme for benthic-to-pelagic transitions in shallow-water fishes<sup>28,59,61</sup> and has also been suggested to be adaptive among demersal deep-sea fishes<sup>13</sup>, elongation in these scenarios is seemingly under selection for sustained swimming (which no anglerfish does). It remains unclear what ecological pressures would select for an elongate body in some anglerfishes but a globular body in others. In summary, future research is needed to determine the relationship between phenotypic and ecological diversity to understand the drivers of evolutionary diversification in the bathypelagic zone and to reconcile deep-sea radiations with predictions of macroevolution developed from other environments<sup>1</sup>.

### The timeline of anglerfish evolution

Our study suggests that the crown age of Lophiiformes may be well within the Cretaceous (Fig. 1), a result that was recently corroborated using UCEs<sup>40</sup>. Yet, previous studies found that Lophiiformes have a Cenozoic origin as part of a post-K–Pg diversification event affecting spiny-rayed fishes broadly<sup>72,121</sup>. We believe that the primary reason for the older age estimates in our study is our use of six fossil calibrations from Monte Bolca, which included crown representatives of Lophioidei and Antennarioidei (Fig. 1). Older age estimates were not limited to analyses using †Plectocretacicoidea, a controversial Cretaceous fossil<sup>79</sup>.

No matter whether Lophiiformes originated before or after the K–Pg boundary, we believe that the ages of lophiiform subclades have been generally underestimated by previous studies. Past studies used at most three Monte Bolca calibrations for Lophiiformes (discussed in detail in Supplementary Appendix 4 and Table 5). This was probably due to lower taxonomic sampling compared with our study, providing fewer

nodes to place calibrations. The fossil record gives no direct evidence of lophiiforms before the Eocene. Yet, the presence of several lineages in Monte Bolca, including crown representatives of two suborders, suggests that Lophiiformes were quite diverse by the early Cenozoic. Branch lengths (in molecular substitution units) at the base of Lophiiformes are not particularly short (Fig. 1 and Supplementary Appendix 1 in ref. 77), suggesting a protracted timeline for diversification.

In a parallel with our study, ref. 74 recently found a Cretaceous crown age of Labridae, another member of the acanthomorphs, using an expanded fossil calibration list compared with past studies. It remains to be seen how an older age of wrasses and anglerfishes would change recent findings of a rapid post-K–Pg radiation of spiny-rayed fishes more generally<sup>72,121</sup>. Regardless, it is clear that improved taxonomic sampling made possible by collections<sup>68</sup> combined with palaeontological systematics<sup>79,96,98</sup> stands to transform our understanding of the timescale of fish evolution.

## Methods

### Data acquisition

We generated genomic data from tissue samples associated with museum specimens (Supplementary Table 1). New data were collected from 152 individuals from 120 species of Lophiiformes. DNA was extracted using the DNeasy Blood and Tissue kit (Qiagen). We shipped DNA extractions to Arbor Biosciences for library preparation, target enrichment and sequencing. Sequencing of paired-end 150-bp reads was completed on a HiSeq 4000 with a total of 192 samples multiplexed per lane. Target capture probes were based on a set of 1,105 single-copy nuclear exon markers designed for fish phylogenomics (Eupercaria bait set of ref. 73). An additional 19 nuclear legacy markers, as well as mitochondrial DNA, were also targeted using this probe set. Information for individuals with new genomic data can be found in Supplementary Table 1. We mined exons from genomes available on NCBI for eight additional outgroup and two ingroup species. Our outgroup sampling (Supplementary Table 1) included 1 holocentrid (representing the sister lineage to Percomorpha), 1 ophidiid (the earliest diverging member of Percomorpha), 1 pelagiarian, 2 syngnatharians, 18 tetraodontiforms and 15 additional eupercarians<sup>75</sup>.

Taxonomic sampling was augmented using two approaches. First, we mined exons from published UCE alignments<sup>71,72</sup>. We assembled the raw reads from these studies into loci using the FishLife Exon Capture pipeline described below. Between 5–357 exons (mean 40.3 per individual) were successfully mined for 93 individuals representing 48 species. After quality control steps, 12 species were retained in the ‘final’ alignment (see below) on the basis of these mined exons. Information for individuals with exons mined from UCEs can be found in Supplementary Table 2. Second, we downloaded legacy markers for 10 species available from NCBI (Supplementary Table 3). These species had between 1 and 5 markers available. Due to the large amounts of missing data introduced in the alignment, we only pursued legacy markers for species that would be new to our dataset. After quality control steps, 2 genera and 6 species not available elsewhere were retained in the ‘final’ alignment on the basis of these legacy markers (Supplementary Table 3).

Our final taxonomic sampling when combining all data, and remaining after all quality control steps (see below), was 132 ingroup species (37.8% of species and 78.1% of genera in Lophiiformes) and 20 of 21 families (all but the monotypic Lophichthyidae). Suborder-level sampling was as follows: 9 species of Lophioidei (32.1% of species and all 4 genera), 21 species of Ogcophaloidei (28.7% of species and 8 of 10 genera), 40 species of Antennarioidei (62.5% of species and 77.3% of genera), 8 species of Chaunacoidei (50% of species and both genera) and 54 species of Ceratioidei (32.1% of species and 74.3% of genera).

### Assembly, alignment and quality control

Assembly, initial raw data quality control steps and alignment were conducted using the FishLife pipelines<sup>73</sup> available at <https://github.com/>

[lilychughes/FishLifeExonCapture](#). Low-quality raw reads and adapter contamination were trimmed using Trimmomatic (v.0.39)<sup>122</sup>. Trimmed reads were mapped against the reference sequences used for probe design with BWA (v.0.7.17)<sup>123</sup>, and PCR duplicates were removed using SAMtools (v.1.9)<sup>124</sup>. An initial sequence for each marker was assembled with Velvet (v.1.2.10)<sup>125</sup>, and the longest contig was used as a reference sequence to extend contigs using aTRAM (2.2)<sup>126</sup> with Trinity (v.2.2) as the assembler<sup>127</sup>. Redundant contigs were excluded with CD-HIT-EST (v.4.8.1)<sup>128,129</sup> and open reading frames for the remaining contigs were identified using Exonerate (v.2.4.0)<sup>130</sup>. Redundant contigs with reading frames exceeding 1% sequence divergence were discarded.

Newly sequenced data, mined exons from UCEs and legacy markers were aligned using MACSE (v.2.03)<sup>131</sup> with the ‘-cleanNonHomologous Sequences’ option. After alignment, we discarded 26 exons with low capture efficiency (those with <50 taxa). Next, some legacy markers can retain paralogues when obtained using our target capture probe set and deserve additional scrutiny<sup>73</sup>. For these markers, we checked their gene trees by eye for pseudogenes. Five exons had pseudogenes (rhodopsin, zic1, sh3px3, plag2 and ENCL) and were excluded from our dataset. After these steps, the dataset contained 1,092 markers. This number included 1,077 FishLife exons, 13 additional nuclear legacy markers and 2 mitochondrial legacy markers (CO1 and ND1).

Further quality control steps followed those described in ref. 132. We performed branch-length correlation (BLC) tests<sup>133</sup> to detect within-gene contamination that may not be easily detectable once genes are concatenated. The logic of this test is that contaminated sequences will show very long branches once constrained to a reference topology. We generated a reference phylogeny using the programme IQ-TREE MPI multicore (v.2.0)<sup>134</sup> on the basis of the concatenated alignment of all 1,092 genes and using mixture models<sup>135</sup>. We then generated gene trees for each marker with the topology constrained to match the reference phylogeny. We generated a branch-length ratio for every taxon in every gene tree, which was the length of the branch in the gene tree over the length of the corresponding branch in the reference tree (after pruning the reference tree to the same individuals as the gene tree). All branches with a ratio >5 were flagged and checked by eye. Ultimately, 1,416 sequences (taxa in gene trees) were discarded from our dataset due to suspected contamination. In addition, two taxa were later dropped entirely from the dataset which had extremely long branches across many gene trees (Supplementary Table 1).

Species identifications of sequences were confirmed using two complimentary approaches. First, for species with more than one individual sampled, we checked the phylogram produced containing all individuals (see below) by eye, with the assumption that species should be monophyletic. Second, we referenced CO1 sequences against the BOLD (Barcode of Life Data System) database<sup>136</sup> using scripts from the ‘fishlifeqc’ package available in GitHub (<https://github.com/Ulises-Rosas/fishlifeqc>). For genera with short branch lengths (specifically, *Ogocephalus*, *Chaunax*, *Oneirodes*, *Gigantactis* and *Himantolophus*), we could not obtain confident species identifications using BOLD, and species were often non-monophyletic. This is potentially due to incomplete lineage sorting after rapid speciation, low substitution rates and/or misidentification. We checked the literature for evidence of ‘taxonomic inflation’ in these genera (in which more species are described from morphology than exist based on molecular divergence) and believed this scenario to potentially apply to *Ogocephalus* and *Himantolophus* (discussed in Supplementary Appendix 2). For individuals outside of these five genera that failed our checks, we checked the voucher specimen whenever possible. This resulted in the re-identification of two museum specimens. We also flagged four previously published sequences from UCE studies as misidentified. If we could not confirm an individual’s identification because there was no CO1 sequence and no conspecific replicate, we referred to the literature to check whether the position of the species in the phylogeny was as expected compared to previous hypotheses,

or at least within the expected genus or family. We preferred to retain individuals for the ‘final’ alignment (see below) for which we could be reasonably confident of their species identification. Quality control results for all individuals can be found in Supplementary Table 1 (new genomic data) and Supplementary Table 2 (individuals taken from UCE alignments).

## Phylogenomic inference

We produced trees from two sets of alignments made from the 1,092-marker dataset. The first ‘all individuals’ set contained all sequences that made it past the BLC step of quality control ( $n = 258$  ingroup individuals). The tree made from this alignment (Supplementary Appendix 1 in ref. 77 and Fig. A1) was checked by eye to confirm the species identity of sequences (for those species with multiple individuals in the dataset) as the final step of quality control (see above). The second ‘final’ alignment was produced by choosing one individual to represent each species ( $n = 132$  ingroup species). When multiple conspecific individuals were available, this representative was always the individual with the greatest number of genes all else being equal (Supplementary Tables 1–3). This ‘final’ alignment was used to produce the phylogenograms used for time calibration and comparative methods. After pruning down to nearly half the number of individuals between the ‘all-individuals’ and the final alignment, genes were un-aligned using the ‘unalign.md’ script within the Goalign toolkit<sup>137</sup>, then re-aligned. The final alignment was 457,635 base pairs long, and alignments for individual markers varied in length from 105–2,682 bp (mean 420 bp).

All 1,092 markers were concatenated using utility scripts in the AMAS package<sup>138</sup>. Trees were constructed with maximum likelihood using the programme IQ-TREE MPI multicore (v.2.0)<sup>134</sup>, implementing mixture models<sup>135</sup> (option -m set to ‘MIX{JC,K2-,HKY,GTR}’). Support was measured using 1,000 ultrafast bootstrap replicates<sup>139</sup> with the ‘-bnni’ option to reduce the risk of overestimating support due to severe model violations.

To account for potential incomplete lineage sorting, we also performed a multispecies coalescent analysis using ASTRAL-II (v.5.7.1)<sup>140</sup> based on gene trees estimated using IQ-TREE with the same settings as above. Nodes within gene trees with bootstrap values <33% were collapsed into polytomies to reduce noise<sup>141</sup>. Support was evaluated using local posterior probabilities<sup>142</sup> (option ‘-t 3’).

## Divergence time estimation

We assembled a list of 21 node calibrations from the literature, including 8 outgroup and 10 ingroup fossil calibrations based on well-preserved articulated skeletal remains, as well as geologic calibrations based on the Isthmus of Panama to constrain the divergence time of three sister-species pairs. Calibration details and justifications are given in Supplementary Appendix 3. Following the recommendations of ref. 143, we established minimum age constraints (that is, the youngest fossil ages) to determine lower bounds for each calibration.

We used two calibration schemes including or excluding the controversial fossil †*Plectocretacicus clarae*, which we placed on the most recent common ancestor of Tetraodontiformes and Lophiiformes<sup>75</sup>. The extinct superfamily †Plectocretacicoidea is purportedly a stem tetraodontiform, and phylogenetic analyses using morphological characters place it as the sister to all remaining Tetraodontiformes<sup>79,144,145</sup>. The earliest plectocretacoid fossils are 94 million years old<sup>144</sup>. Therefore, due to the apical position of Tetraodontiformes within acanthomorphs and the sister-group relationship between Tetraodontiformes and Lophiiformes, this calibration has potential to greatly increase the age of early nodes in the phylogeny of Lophiiformes. However, some authors do not believe †Plectocretacicoidea are related to Tetraodontiformes, or at least that the evidence for this relationship is unconvincing<sup>121,146–148</sup>.

We produced eight alternative time trees using either the IQ-TREE (concatenated) or ASTRAL (summary coalescent species) trees, the

fossil calibration scheme with or without *Plectocretacicus*, and using either MCMCTree or RelTime as the calibration method. Both MCMCTree and RelTime can handle genomic-scale datasets, but these approaches are otherwise quite different. MCMCTree uses a birth-death tree prior and an independent rates clock model in which rates follow a log-normal distribution in a Bayesian framework<sup>80,81</sup>. RelTime does not use priors on lineage rates and instead computes relative time and lineage rates directly from branch lengths in the phylogram (the ‘relative rate framework’)<sup>82,83</sup>. Note that RelTime tends to underestimate divergence times for branches with very few molecular substitutions, unlike methods that include a tree prior<sup>149,150</sup>.

For MCMCTree, fossil calibrations used uniform distributions and geologic calibrations used Cauchy distributions (Supplementary Appendix 3 and Table A3). We estimated distribution densities for the upper age of clades based on the algorithm proposed in ref. 151. This approach uses a list of fossil outgroup age records based on the oldest minima to produce a probable distribution of the origin of a given clade (details in Supplementary Appendix 3). From the distribution estimated for each calibration, we extracted the 95% confidence interval to set the soft upper bound (maximum age) for MCMCTree, and to calculate the unitless mean and standard deviation for log-normal distributions for RelTime.

We implemented MCMCTree analyses using the PAML (v.4.9h) package<sup>152</sup>. We divided the alignment into two partitions: 1st and 2nd codon position, and 3rd codon position. We used the HKY85 substitution model and the independent rate relaxed clock model. Additional prior parameters were set as follows: BDparas: 1, 1, 0.38; kappa\_gamma: 6, 2; alpha\_gamma=1, 1; rgene\_gamma=2, 200, 1; sigma2\_gamma=2, 5, 1. To improve computation time, we first used the approximate method to calculate the likelihood<sup>81</sup>. Markov chain Monte Carlo (MCMC) chains were run twice independently for 20 or 30 million generations as needed to converge (number of samples=200,000, sample frequency=100 or 150, and burnin=2,000). We used Tracer (v.1.7.1)<sup>153</sup> to check for convergence.

RelTime uses a maximum-likelihood framework implemented in the software MEGAX<sup>154</sup>. For the IQ-TREEs, we applied the RelTime-branch lengths approach, employing a maximum relative rate ratio of 20, with the tree topology serving as the input. For the ASTRAL trees, we used RelTime-ML with the GTR + I model while maintaining the default settings to optimize branch lengths. The ASTRAL topology and the concatenated alignment were used as inputs. This was necessary because the ASTRAL tree was made from gene trees and not estimated directly from the alignment.

### Ancestral habitat and lineage diversification rates

Following ref. 56, we used BioGeoBEARS (v.1.1.3)<sup>155</sup> to infer ancestral habitats. This approach allowed us to code species as occurring in more than one ‘region’. Our analysis included three regions: benthic continental shelf (that is, benthic in shallow-water environments), benthic continental slope to abyssal plain (that is, benthic in deep-sea environments) and deep-sea pelagic. Habitats were coded on the basis of FishBase<sup>156</sup>, Fishes of Australia<sup>157</sup> and refs. 12,28 (Supplementary Table 4). The maximum number of regions allowed per species was set to two. We compared the fit of six alternative models using corrected Akaike information criterion (AICc) weights<sup>158</sup>. These models were: DEC<sup>159</sup>, DIVA-LIKE<sup>160</sup>, BAYAREA-LIKE<sup>161</sup> and their equivalents with the +J parameter (Supplementary Table 5). We performed these analyses on all eight trees to use as input for OUwie (see below).

We estimated lineage diversification rates using the MiSSE<sup>85</sup> framework implemented in the hisse R package (v.2.1.1). MiSSE operates like HiSSE<sup>162</sup> but does not consider the influence of any characters chosen by the researcher, instead modelling rate shifts agnostic of a priori hypotheses. We performed analyses for all eight trees individually. We were concerned that taxonomic inflation could inflate speciation rates in the genera *Himantolophus* and *Ogcocephalus* (Supplementary

Appendix 2). Therefore, we also performed analyses on a set of eight trees with these genera pruned to two species (to retain the crown age) (Supplementary Table 6). We compared the fit of models with 1–10 rate classes, setting a global sampling fraction of 38%. Following recommended practices<sup>80</sup>, we model-averaged the rates inferred from models with >5% of the AICc weight, where the contribution of each model towards the mean was proportional to its Akaike weight. We plotted model-averaged rates onto the branches of the tree using the gghisce package (v.0.1.1)<sup>163</sup>. It is believed that State-Dependent Speciation and Extinction models avoid issues of identifiability raised in ref. 164 because they incorporate multiple information sources to infer rates<sup>165</sup>.

### Phenotypic datasets

Body shape was measured using linear measurements taken from intact alcohol-preserved adults from museum collections using digital calipers with a minimum resolution of 0.1 mm. We took eight measurements following ref. 94 (standard length, maximum body depth, maximum fish width, head depth, lower jaw length, mouth width, minimum caudal peduncle depth and minimum caudal peduncle width) plus two additional measurements (eye diameter and interorbital distance). No male ceratioids were used. Measurements are illustrated in Extended Data Fig. 7.

Linear measurements were size corrected using two approaches following refs. 35,94. First, we used log-shape ratios<sup>166</sup>: each variable was divided by the geometric mean of standard length, maximum body depth and maximum fish width, and then log transformed. The mean and standard error of each trait for each species were used in downstream analyses. Second, we took the residuals from a PGLS of each trait (species means after log transformation) against the geometric mean size. Each PGLS was performed using the ‘procD.pgls’ function from the geomorph R package (v.4.0.5)<sup>167</sup> with 10,000 iterations to assess significance. All eight trees were used alternatively as the input tree. Each approach to size correction has benefits and disadvantages. We could estimate the standard error for use with other analyses (Extended Data Fig. 10) using log-shape ratios, but not using PGLS (because the regression requires species mean traits as the input data, so we needed to take means before size correction). On the other hand, PGLS residuals remove variation due to allometry.

For quality control, we flagged measurements that were outside the interquartile range for the genus (after size correction with log-shape ratios) and specimens with flags were excluded. The final dataset after quality control contained measurements for 331 individuals from 113 species (representing 85.6% of tips in the phylogeny), in which 1–9 individuals per species were measured (mean of 2.9 and median of 2 individuals per species). For the subset of species with >2 specimens measured, we statistically compared standard errors of each trait (a measure of intraspecific variation) across suborders using analysis of variance (ANOVA) with a post hoc pairwise Tukey test implemented with the multcomp R package (v.1.4–25)<sup>168</sup>. If ceratioids are more prone to preservation artefacts and specimen damage than other lophiiforms, then this should manifest as greater standard error around species means. Standard errors were significantly different across suborders for six of ten traits, but ceratioids did not always have the highest errors, contrary to expectation. Instead, errors were distributed idiosyncratically for each trait (Extended Data Fig. 10).

Skull shape was measured using three-dimensional geometric morphometrics collected from µCT scans<sup>169</sup> of alcohol-preserved museum specimens of intact adult anglerfishes. Scans were collected at the Karel F. Liem Bio-Imaging Center at the University of Washington Friday Harbor Laboratories and Rice University. Skulls were segmented using Amira (v.2020.3)<sup>170</sup> and exported as mesh files. Mesh files were digitized with 111 three-dimensional landmarks (41 point and 70 semi-sliding; Extended Data Fig. 4) in the software Stratovan Checkpoint<sup>171</sup>. Landmarks were treated as bilaterally symmetrical and thus only placed on the left side of the skull<sup>172–174</sup>. Our µCT scan dataset

contained 100 species of Lophiiformes ( $n = 1$  scan per species) representing 75.7% of the tips in our phylogeny (Supplementary Table 7). Of these, 38 are new to this study, 33 were previously published<sup>114</sup> and 29 were downloaded from the online repositories MorphoSource (<https://www.morphosource.org/>) and Virtual Natural History Museum (<http://vnhm.de/VNHM/index.php>). Due to the high mobility of cranial elements in fish skulls<sup>173,174</sup>, to reduce the influence of preservation artefacts on shape variation we performed a local superimposition to standardize the position of individual skull elements<sup>175</sup> before any downstream analyses.

We performed analyses using four multivariate datasets: body shape (linear measurements size corrected with either log-shape ratios or PGLS residuals), whole skulls and the oral jaws, with the latter two being based on  $\mu$ CT scans. To quantify jaw shape, we isolated the 41 (13 point and 28 semi-sliding; Extended Data Fig. 4) landmarks placed on the premaxilla, angular and dentary. The same bones were isolated in ref. 114 in their analysis of anglerfish jaw and tooth shape using linear measurements.

### Phenotypic evolution

We visualized shape variation using a phylomorphospace analysis<sup>176</sup> performed with the function ‘gm.prcomp’ in the geomorph package<sup>167</sup>. We calculated disparity within each habitat category (shallow benthic, shallow and deep benthic, deep benthic and deep pelagic) using a test of morphological partial disparities for the overall mean<sup>87</sup> implemented with the ‘morphol.disparity’ function in geomorph. Pairwise significance among categories was assessed with 10,000 iterations. We assessed disparity for the four multivariate datasets, as well as for each of the ten body shape measurements individually (repeated for each size-correction strategy). We observed that disparity in eye diameter was high for ceratioids (Extended Data Figs. 7 and 9) even though they visually appear to have small eyes regardless of body shape or size (Fig. 6). Therefore, we also calculated disparity for eye diameter without size correction to ensure that disparity was not being introduced when size-correcting by geometric mean size. Ceratioids still had high disparity in log-transformed eye diameter relative to other lophiiforms before size correction (Supplementary Appendix 5 in ref. 77), suggesting that this result is not artefactual.

In the age of ‘phenomics’, the average size of multivariate phenotypic datasets is outpacing the development of statistical approaches<sup>177–180</sup>. We used the variable-rates model<sup>93</sup> implemented within BayesTraits (v.4)<sup>88</sup> to infer temporal shifts in evolutionary rates, following recent studies of complex multivariate datasets across vertebrate clades<sup>89,90,181</sup>. This approach allows the Brownian rate of evolution ( $\sigma^2$ ) to vary along branches of the phylogeny without an a priori expectation of their location. Therefore, this approach accommodates the complex evolutionary dynamics we expected, given the large phenotypic diversity observed across Lophiiformes and within subclades (Fig. 3). Given the limited options for evolutionary model comparison appropriate for multivariate datasets<sup>178,179</sup>, the BayesTraits software allows for fitting user-defined models by specifying transformations of the input tree according to predictions of different evolutionary scenarios<sup>88</sup>, which are then analysed under the variable-rates framework<sup>93</sup>. For example, a multiple-optima OU model<sup>182</sup> can be fit by specifying local branch-length transformations to regions of the phylogeny associated with different habitats (‘LocalTransform’ option<sup>88</sup>). We chose this approach for its flexibility but give two caveats. First, tree transformations generated under different underlying evolutionary scenarios can appear similar<sup>88</sup>. Therefore, we focused on interpreting a range of parameter estimates over interpreting a single best-fitting model, following best practices in phylogenetic comparative methods<sup>86,183,184</sup>. Second, scalar values reflect both the rate of evolution and local transformations (when used), making inferences based on these models more difficult to interpret. For this reason, we interpreted results from analyses using

these local transformations alongside those from simpler models and looked for commonalities.

Variable-rate models were fit using a reversible-jump MCMC procedure to sample parameters along the phylogeny. To assess the mode of evolution, we used Bayes Factors to weigh support for four alternative models, each with single or variable-rate options, for a total of eight models: Brownian motion, early burst (‘delta’ tree transformation), OU with a single optimum across Lophiiformes and multiple-peak OU with different optima associated with the four habitat states. To fit OU models, the software transforms the input tree according to an ‘OU parameter’<sup>88</sup> that measures the strength of return to the optimum (analogous to the  $\alpha$  parameter of OUwie<sup>185</sup>). The value(s) of this parameter for each optimum is inferred as part of the rjMCMC procedure; values  $> 0$  indicate an OU process, with increasing values indicating stronger selection. As input, we used PC scores for the number of axes summing to 95% (body shape) or 85% (skull and jaws) of the variance. This number was 6 axes for body shape, 28 axes for skull shape and 12 axes for jaw shape. We only used the number of axes summing to 85% of the variance for the  $\mu$ CT scan data because a large number of additional PC axes accounted for little individual variance while inflating computational load (specifically, 51 PC axes added up to 95% of variation in skull shape). Our analyses investigated evolution in body (both size-correction strategies), skull and jaw shape using two alternative trees (IQ-TREE without †*Plectocretacicus* calibrated using either MCMCTree or RelTime), for eight sets of analyses. We chose these two trees because other analyses demonstrated that the choice of time calibration method had the strongest influence on comparative inferences (for example, Fig. 1 and Extended Data Fig. 2). Following software recommendations<sup>88</sup>, we used the BayesTraits setting ‘TestCorrel’ to constrain the correlation between PC axes to zero, because multivariate analyses require independence of traits. Chains were run for 200–350 million generations with a burnin of 30%. A stepping-stone sampler was used to estimate the marginal likelihood with 50 stones to run for 1,400,000 generations after convergence. Analyses were run twice and convergence of the runs was confirmed on the basis of trace plots and Gelman diagnostics near 1 using the R package coda (v.0.1.9–4)<sup>186</sup>.

The output of variable-rate analyses is a posterior distribution of phylogenies where each branch is scaled by the degree of phenotypic change: branches with scalars  $< 1$  are compressed relative to the input tree scaled by time units, while branches with scalars  $> 1$  are lengthened. This provides a means of visualizing evolutionary shifts across the phylogeny<sup>93</sup>. Under a Brownian motion model, the scalar reflects the evolutionary rate  $\sigma^2$ . Under a model with local transformations, scalars reflect both the evolutionary rate and the transformation parameter and can therefore be difficult to interpret. To aid interpretation, we plotted scalars estimated from two underlying models: a multi-optima OU model (the best-fitting model under most circumstances) and a Brownian motion model which lacks the complication of intertwining local transformations with the rate scalars (Extended Data Fig. 6). BayesTraits output was processed using utility functions from the packages BTProcessR (v.0.0.1)<sup>187</sup> and BTRTools (0.0.0.9)<sup>188</sup>.

To evaluate the effects of selection on different aspects of phenotypes, we fit evolutionary models on the ten univariate body shape variables individually using the OUwie R package (v.2.10)<sup>184,185</sup>. For each trait, we compared the fit of six models using AICc weights: single-rate Brownian, multiple-rate Brownian, single-peak and single-rate OU, multiple-peak OU with different optima for each habitat but a single evolutionary rate, multiple-peak and multiple-rate ( $\sigma^2$ ) OU, and multiple-peak and multiple-alpha ( $\alpha$ ) OU but a single rate. We input a phylogeny with nodes annotated with the most-likely habitat state inferred by BioGeoBEARS (Extended Data Fig. 1); all eight trees and corresponding BioGeoBEARS results were used as alternatives. When using variables size corrected using log-shape ratios, we also input the standard error of the species mean using the option ‘mserr=“known”’ (Extended Data Fig. 10).

## Reporting summary

Further information on research design is available in the Nature Portfolio Reporting Summary linked to this article.

## Data availability

Raw sequence reads have been archived in the NCBI Sequence Read Archive with the BioProject number PRJNA1074427. Any pre-existing sequence data used are given in Supplementary Tables 2 and 3 with accession codes. All CT scans are publicly available on Morphosource (<https://www.morphosource.org/>) with media numbers in Supplementary Table 7. Time-calibrated phylogenies and body shape dataset are available in DRYAD<sup>77</sup>.

## Code availability

Pipelines for genomic assembly are available in GitHub<sup>189</sup>. R scripts and inputs needed to replicate analyses are available in DRYAD<sup>77</sup>.

## References

1. Gillespie, R. G. et al. Comparing adaptive radiations across space, time, and taxa. *J. Hered.* **111**, 1–20 (2020).
2. Schlüter, D. *The Ecology of Adaptive Radiation* (Oxford Univ. Press, 2000).
3. Yoder, J. B. et al. Ecological opportunity and the origin of adaptive radiations. *J. Evol. Biol.* **23**, 1581–1596 (2010).
4. Stroud, J. T. & Losos, J. B. Ecological opportunity and adaptive radiation. *Annu. Rev. Ecol. Evol. Syst.* **47**, 507–532 (2016).
5. Evans, K. M., Larouche, O., West, J. L., Gartner, S. M. & Westneat, M. W. Burrowing constrains patterns of skull shape evolution in wrasses. *Evol. Dev.* **25**, 73–84 (2022).
6. Burress, E. D. & Hart, P. B. Pelagic zone is an evolutionary catalyst, but an ecological dead end, for North American minnows. *Evolution* **78**, 1396–1404 (2024).
7. Marshall, N. B. *Explorations in the Life of Fishes* (Harvard Univ. Press, 1971).
8. Childress, J. J. Are there physiological and biochemical adaptations of metabolism in deep-sea animals? *Trends Ecol. Evol.* **10**, 30–36 (1995).
9. McClain, C. R. & Hardy, S. M. The dynamics of biogeographic ranges in the deep sea. *Proc. R. Soc. B* **277**, 3533–3546 (2010).
10. Woolley, S. N. C. et al. Deep-sea diversity patterns are shaped by energy availability. *Nature* **533**, 393–396 (2016).
11. Cowles, D. L. & Childress, J. J. Aerobic metabolism of the anglerfish *Melanocetus johnsoni*, a deep-pelagic marine sit-and-wait predator. *Deep Sea Res. I* **42**, 1631–1638 (1995).
12. Pietsch, T. W. *Oceanic Anglerfishes: Extraordinary Diversity in the Deep Sea* (Univ. of California Press, 2009).
13. Neat, F. C. & Campbell, N. Proliferation of elongate fishes in the deep sea. *J. Fish. Biol.* **83**, 1576–1591 (2013).
14. Sutton, T. T. Vertical ecology of the pelagic ocean: classical patterns and new perspectives. *J. Fish. Biol.* **83**, 1508–1527 (2013).
15. Drazen, J. C. & Sutton, T. T. Dining in the deep: the feeding ecology of deep-sea fishes. *Annu. Rev. Mar. Sci.* **9**, 337–366 (2017).
16. Priede, I. G. *Deep-Sea Fishes: Biology, Diversity, Ecology and Fisheries* (Cambridge Univ. Press, 2017).
17. de Busserolles, F., Fogg, L., Cortesi, F. & Marshall, J. The exceptional diversity of visual adaptations in deep-sea teleost fishes. *Semin. Cell Dev. Biol.* **106**, 20–30 (2020).
18. Gerringer, M. E. et al. Habitat influences skeletal morphology and density in the snailfishes (family Liparidae). *Front. Zool.* **18**, 16 (2021).
19. McGonagle, R. P., Kerstetter, D. W., Fenolio, D. & Sutton, T. T. Ecomorphology of a predatory deep-sea fish family: does trophic specialization drive hyperspeciation? *Front. Mar. Sci.* **10**, 1056094 (2023).
20. Myers, E. M. V., Anderson, M. J., Eme, D., Liggins, L. & Roberts, C. D. Changes in key traits versus depth and latitude suggest energy-efficient locomotion, opportunistic feeding and light lead to adaptive morphologies of marine fishes. *J. Anim. Ecol.* **89**, 309–322 (2020).
21. Gray, J. S. Marine biodiversity: patterns, threats and conservation needs. *Biodivers. Conserv.* **6**, 153–175 (1997).
22. Gratwicke, B. & Speight, M. R. The relationship between fish species richness, abundance and habitat complexity in a range of shallow tropical marine habitats. *J. Fish. Biol.* **66**, 650–667 (2005).
23. Alfaro, M. E., Santini, F. & Brock, C. D. Do reefs drive diversification in marine teleosts? Evidence from the pufferfish and their allies (order Tetraodontiformes). *Evolution* **61**, 2104–2126 (2007).
24. Kiessling, W., Simpson, C. & Foote, M. Reefs as cradles of evolution and sources of biodiversity in the Phanerozoic. *Science* **327**, 196–198 (2010).
25. Price, S. A., Holzman, R., Near, T. J. & Wainwright, P. C. Coral reefs promote the evolution of morphological diversity and ecological novelty in labrid fishes. *Ecol. Lett.* **14**, 462–469 (2011).
26. Burress, E. D. & Wainwright, P. C. Adaptive radiation in labrid fishes: a central role for functional innovations during 65 My of relentless diversification. *Evolution* **73**, 346–359 (2019).
27. Evans, K. M., Williams, K. L. & Westneat, M. W. Do coral reefs promote morphological diversification? Exploration of habitat effects on labrid pharyngeal jaw evolution in the era of big data. *Integr. Comp. Biol.* **59**, 696–704 (2019).
28. Friedman, S. T. et al. Body shape diversification along the benthic–pelagic axis in marine fishes. *Proc. R. Soc. B* **287**, 20201053 (2020).
29. Corn, K. A. et al. The rise of biting during the Cenozoic fueled reef fish body shape diversification. *Proc. Natl Acad. Sci. USA* **119**, e2119828119 (2022).
30. Jablonski, D. Evolvability and macroevolution: overview and synthesis. *Evol. Biol.* **49**, 265–291 (2022).
31. Frédéric, B., Marramà, G., Carnevale, G. & Santini, F. Non-reef environments impact the diversification of extant jacks, remoras and allies (Carangoidei, Percormorpha). *Proc. R. Soc. B* **283**, 20161556 (2016).
32. Larouche, O. et al. Reef-associated fishes have more maneuverable body shapes at a macroevolutionary scale. *Coral Reefs* **39**, 1427–1439 (2020).
33. Maile, A. J., May, Z. A., DeArmon, E. S., Martin, R. P. & Davis, M. P. Marine habitat transitions and body-shape evolution in lizardfishes and their allies (Aulopiformes). *Copeia* **108**, 820–832 (2020).
34. Carrington, V. G. et al. How functionally diverse are fish in the deep? A comparison of fish communities in deep and shallow-water systems. *Divers. Distrib.* **27**, 1208–1223 (2021).
35. Martinez, C. M. et al. The deep sea is a hot spot of fish body shape evolution. *Ecol. Lett.* **24**, 1788–1799 (2021).
36. May, R. M. Biological diversity: differences between land and sea. *Phil. Trans. Biol. Sci.* **343**, 105–111 (1994).
37. Angel, M. V. & Boxshall, G. A. Life in the benthic boundary layer: connections to the mid-water and sea floor [and discussion]. *Phil. Trans. R. Soc. Lond. A* **331**, 15–28 (1990).
38. Pietsch, T. W. in *Ontogeny and Systematics of Fishes* (eds Moser, H. G. et al.) 320–325 (American Society of Ichthyologists and Herpetologists, 1984).
39. Swann, J. B., Holland, S. J., Petersen, M., Pietsch, T. W. & Boehm, T. The immunogenetics of sexual parasitism. *Science* **369**, 1608–1615 (2020).
40. Brownstein, C. D. et al. Synergistic innovations enabled the radiation of anglerfishes in the deep open ocean. *Curr. Biol.* **34**, 2541–2550.e4 (2024).
41. Pietsch, T. W. & Arnold, R. J. *Frogfishes: Biodiversity, Zoogeography, and Behavioral Ecology* (John Hopkins Univ. Press, 2020).

42. Dickson, B. V. & Pierce, S. E. How (and why) fins turn into limbs: insights from anglerfish. *Earth Environ. Sci. Trans. R. Soc. Edinb.* **109**, 87–103 (2018).
43. Farina, S. C. & Bernis, W. E. Functional morphology of gill ventilation of the goosefish, *Lophius americanus* (Lophiiformes: Lophiidae). *Zoology* **119**, 207–215 (2016).
44. Long, N. P. & Farina, S. C. Enormous gill chambers of deep-sea coffinfishes (Lophiiformes: Chaunacidae) support unique ventilatory specialisations such as breath holding and extreme inflation. *J. Fish. Biol.* **95**, 502–509 (2019).
45. Farina, S. C., Near, T. J. & Bernis, W. E. Evolution of the branchiostegal membrane and restricted gill openings in Actinopterygian fishes. *J. Morphol.* **276**, 681–694 (2015).
46. Sanders, H. L. Marine benthic diversity: a comparative study. *Am. Nat.* **102**, 243–282 (1968).
47. Caruso, J. H., Ross, S. W., Sulak, K. J. & Sedberry, G. R. Deep-water chaunacid and lophiid anglerfishes (Pisces: Lophiiformes) off the south-eastern United States. *J. Fish. Biol.* **70**, 1015–1026 (2007).
48. Lundsten, L., Johnson, S. B., Cailliet, G. M., DeVogelaere, A. P. & Clague, D. A. Morphological, molecular, and in situ behavioral observations of the rare deep-sea anglerfish *Chaunacops coloratus* (Garman, 1899), order Lophiiformes, in the eastern North Pacific. *Deep Sea Res. I* **68**, 46–53 (2012).
49. Pietsch, T. W., Ross, S. W., Caruso, J. H., Saunders, M. G. & Fisher, C. R. In situ observations of the deep-sea goosefish *Sladenia shaefersi* Caruso and Bullis (Lophiiformes: Lophiidae), with evidence of extreme sexual dimorphism. *Copeia* **2013**, 660–665 (2013).
50. Palumbi, S. R. Marine speciation on a small planet. *Trends Ecol. Evol.* **7**, 114–118 (1992).
51. Norris, R. D. Pelagic species diversity, biogeography, and evolution. *Paleobiology* **26**, 236–258 (2000).
52. Gaither, M. R., Bowen, B. W., Rocha, L. A. & Briggs, J. C. Fishes that rule the world: circumtropical distributions revisited. *Fish Fish.* **17**, 664–679 (2016).
53. Miya, M. & Nishida, M. Speciation in the open ocean. *Nature* **389**, 803–804 (1997).
54. Yamanoue, Y. et al. Explosive speciation of *Takifugu*: another use of fugu as a model system for evolutionary biology. *Mol. Biol. Evol.* **26**, 623–629 (2008).
55. Denton, J. S. S. Diversification patterns of lanternfishes reveal multiple rate shifts in a critical mesopelagic clade targeted for human exploitation. *Curr. Biol.* **28**, 933–940 (2018).
56. Miller, E. C. et al. Alternating regimes of shallow and deep-sea diversification explain a species-richness paradox in marine fishes. *Proc. Natl Acad. Sci. USA* **119**, e2123544119 (2022).
57. Childress, J. J. & Mickel, T. J. Metabolic rates of animals from the hydrothermal vents and other deep-sea habitats. *Bull. Biol. Soc. Wash.* **6**, 249–260 (1985).
58. Collar, D. C., O'Meara, B. C., Wainwright, P. C. & Near, T. J. Piscivory limits diversification of feeding morphology in centrarchid fishes. *Evolution* **63**, 1557–1573 (2009).
59. Friedman, S. T., Price, S. A., Hoey, A. S. & Wainwright, P. C. Ecomorphological convergence in planktivorous surgeonfishes. *J. Evol. Biol.* **29**, 965–978 (2016).
60. Friedman, M. et al. A phylogenomic framework for pelagician fishes (Acanthomorpha: Percomorpha) highlights mosaic radiation in the open ocean. *Proc. R. Soc. B* **286**, 20191502 (2019).
61. Rincon-Sandoval, M. et al. Evolutionary determinism and convergence associated with water-column transitions in marine fishes. *Proc. Natl Acad. Sci. USA* **117**, 33396–33403 (2020).
62. McCune, A. R. Evolutionary novelty and atavism in the *Semionotus* complex: relaxed selection during colonization of an expanding lake. *Evolution* **44**, 71–85 (1990).
63. Glor, R. E. Phylogenetic insights on adaptive radiation. *Annu. Rev. Ecol. Evol. Syst.* **41**, 251–270 (2010).
64. Losos, J. B. Adaptive radiation, ecological opportunity, and evolutionary determinism. *Am. Nat.* **175**, 623–639 (2010).
65. Davis, M. P., Midford, P. E. & Maddison, W. Exploring power and parameter estimation of the BiSSE method for analyzing species diversification. *BMC Evol. Biol.* **13**, 38 (2013).
66. Webb, T. J., Vanden Berghe, E. & O'Dor, R. Biodiversity's big wet secret: the global distribution of marine biological records reveals chronic under-exploration of the deep pelagic ocean. *PLoS ONE* **5**, e10223 (2010).
67. Lutj, W. B. & Clardy, T. R. First detection of biofluorescence in a deep-sea anglerfish. *J. Fish. Biol.* **100**, 843–846 (2022).
68. Card, D. C., Shapiro, B., Giribet, G., Moritz, C. & Edwards, S. V. Museum genomics. *Annu. Rev. Genet.* **55**, 633–659 (2021).
69. Maslenikov, K. P. Specimens by the millions: managing large, specialized collections at the University of Washington Burke Museum Fish Collection. *Ichthyol. Herpetol.* **109**, 397–406 (2021).
70. Miya, M. et al. Evolutionary history of anglerfishes (Teleostei: Lophiiformes): a mitogenomic perspective. *BMC Evol. Biol.* **10**, 58 (2010).
71. Hart, P. B. et al. Evolutionary relationships of anglerfishes (Lophiiformes) reconstructed using ultraconserved elements. *Mol. Phylogenet. Evol.* **171**, 107459 (2022).
72. Ghezelayagh, A. et al. Prolonged morphological expansion of spiny-rayed fishes following the end-Cretaceous. *Nat. Ecol. Evol.* **6**, 1211–1220 (2022).
73. Hughes, L. C. et al. Exon probe sets and bioinformatics pipelines for all levels of fish phylogenomics. *Mol. Ecol. Resour.* **21**, 816–833 (2021).
74. Hughes, L. C., Nash, C. M., White, W. T. & Westneat, M. W. Concordance and discordance in the phylogenomics of the wrasses and parrotfishes (Teleostei: Labridae). *Syst. Biol.* **72**, 530–543 (2022).
75. Troyer, E. M. et al. The impact of paleoclimatic changes on body size evolution in marine fishes. *Proc. Natl Acad. Sci. USA* **119**, e2122486119 (2022).
76. Rabosky, D. L. et al. An inverse latitudinal gradient in speciation rate for marine fishes. *Nature* **559**, 392–395 (2018).
77. Miller, Elizabeth. Data and R scripts for "Reduced evolutionary constraint accompanies ongoing radiation in deep-sea anglerfishes". DRYAD <https://doi.org/10.5061/dryad.n2z34tn5r> (2024).
78. Friedman, M. & Carnevale, G. The Bolca Lagerstätten: shallow marine life in the Eocene. *J. Geol. Soc.* **175**, 569–579 (2018).
79. Arcila, D. & Tyler, J. C. Mass extinction in tetraodontiform fishes linked to the Palaeocene–Eocene thermal maximum. *Proc. R. Soc. B* **284**, 20171771 (2017).
80. Rannala, B. & Yang, Z. Inferring speciation times under an episodic molecular clock. *Syst. Biol.* **56**, 453–466 (2007).
81. dos Reis, M. & Yang, Z. in *Evolutionary Genomics: Statistical and Computational Methods* (ed. Anisimova, M.) 309–330 (Springer, 2019).
82. Tamura, K. et al. Estimating divergence times in large molecular phylogenies. *Proc. Natl Acad. Sci. USA* **109**, 19333–19338 (2012).
83. Tamura, K., Tao, Q. & Kumar, S. Theoretical foundation of the RelTime method for estimating divergence times from variable evolutionary rates. *Mol. Biol. Evol.* **35**, 1770–1782 (2018).
84. Colmenero, A., Aguzzi, J., Lombarte, A. & Bozzano, A. Sensory constraints in temporal segregation in two species of anglerfish, *Lophius budegassa* and *L. piscatorius*. *Mar. Ecol. Prog. Ser.* **416**, 255–265 (2010).
85. Vasconcelos, T., O'Meara, B. C. & Beaulieu, J. M. A flexible method for estimating tip diversification rates across a range of speciation and extinction scenarios. *Evolution* **76**, 1420–1433 (2022).
86. Caetano, D. S., O'Meara, B. C. & Beaulieu, J. M. Hidden state models improve state-dependent diversification approaches,

- including biogeographical models. *Evolution* **72**, 2308–2324 (2018).
87. Foote, M. Contributions of individual taxa to overall morphological disparity. *Paleobiology* **19**, 403–419 (1993).
  88. Meade, A. & Pagel, M. BayesTraits V4. <http://www.evolution.reading.ac.uk/BayesTraitsV4.0.1/BayesTraitsV4.0.1.html> (Reading Evolutionary Biology Group, 2023).
  89. Goswami, A. et al. Attenuated evolution of mammals through the Cenozoic. *Science* **378**, 377–383 (2022).
  90. Buser, T. J. et al. Freshwater habitats promote rapid rates of phenotypic evolution in sculpin fishes (Perciformes: Cottoidea). *Am. Nat.* **204**, 345–360 (2024).
  91. Simpson, G. G. *Tempo and Mode in Evolution* (Columbia Univ. Press, 1944).
  92. Slater, G. J. & Friscia, A. R. Hierarchy in adaptive radiation: a case study using the Carnivora (Mammalia). *Evolution* **73**, 524–539 (2019).
  93. Venditti, C., Meade, A. & Pagel, M. Multiple routes to mammalian diversity. *Nature* **479**, 393–396 (2011).
  94. Price, S. A. et al. Building a body shape morphospace of teleostean fishes. *Integr. Comp. Biol.* **59**, 716–730 (2019).
  95. Carnevale, G. & Pietsch, T. W. An Eocene frogfish from Monte Bolca, Italy: the earliest known skeletal record for the family. *Palaeontology* **52**, 745–752 (2009).
  96. Carnevale, G. & Pietsch, T. W. Eocene handfishes from Monte Bolca, with description of a new genus and species, and a phylogeny of the family Brachionichthyidae (Teleostei: Lophiiformes). *Zool. J. Linn. Soc.* **160**, 621–647 (2010).
  97. Carnevale, G. & Pietsch, T. W. Batfishes from the Eocene of Monte Bolca. *Geol. Mag.* **148**, 461–472 (2011).
  98. Carnevale, G. & Pietsch, T. W. *tCaruso*, a new genus of anglerfishes from the Eocene of Monte Bolca, Italy, with a comparative osteology and phylogeny of the teleost family Lophiidae. *J. Syst. Paleontol.* **10**, 47–72 (2012).
  99. Pietsch, T. W. & Carnevale, G. A new genus and species of anglerfish (Teleostei: Lophiiformes: Lophiidae) from the Eocene of Monte Bolca, Italy. *Copeia* **2011**, 64–71 (2011).
  100. Carnevale, G., Pietsch, T. W., Bonde, N., Leal, M. E. C. & Marramà, G. *#Neilpearlia ceratoi*, gen. et sp. nov., a new frogfish from the Eocene of Bolca, Italy. *J. Vertebr. Paleontol.* **40**, e1778711 (2020).
  101. Price, S. A., Tavera, J. J., Near, T. J. & Wainwright, P. C. Elevated rates of morphological and functional diversification in reef-dwelling haemulid fishes. *Evolution* **67**, 417–428 (2013).
  102. Sallan, L., Friedman, M., Sansom, R. S., Bird, C. M. & Sansom, I. J. The nearshore cradle of early vertebrate diversification. *Science* **362**, 460–464 (2018).
  103. Jablonski, D., Sepkoski, J. J., Bottjer, D. J. & Sheehan, P. M. Onshore–offshore patterns in the evolution of Phanerozoic shelf communities. *Science* **222**, 1123–1125 (1983).
  104. Evans, K. M. et al. Beaks promote rapid morphological diversification along distinct evolutionary trajectories in labrid fishes (Eupercaria: Labridae). *Evolution* **77**, 2000–2014 (2023).
  105. Todd Streelman, J. & Danley, P. D. The stages of vertebrate evolutionary radiation. *Trends Ecol. Evol.* **18**, 126–131 (2003).
  106. Wainwright, P. C. & Price, S. A. The impact of organismal innovation on functional and ecological diversification. *Integr. Comp. Biol.* **56**, 479–488 (2016).
  107. Schwenk, K. & Wagner, G. N. P. Function and the evolution of phenotypic stability: connecting pattern to process. *Am. Zool.* **41**, 552–563 (2001).
  108. Buser, T. J., Finnegan, D. L., Summers, A. P. & Kolmann, M. A. Have niche, will travel. New means of linking diet and ecomorphology reveals niche conservatism in freshwater cottoid fishes. *Integr. Org. Biol.* **1**, obz023 (2019).
  109. Olson, M. E. & Arroyo-Santos, A. Thinking in continua: beyond the “adaptive radiation” metaphor. *BioEssays* **31**, 1337–1346 (2009).
  110. Czekanski-Moir, J. E. & Rundell, R. J. The ecology of non-ecological speciation and non-adaptive radiations. *Trends Ecol. Evol.* **34**, 400–415 (2019).
  111. Moen, D. S., Ravelojaona, R. N., Hutter, C. R. & Wiens, J. J. Testing for adaptive radiation: a new approach applied to Madagascar frogs. *Evolution* **75**, 3008–3025 (2021).
  112. Hutchinson, G. E. The paradox of the plankton. *Am. Nat.* **95**, 137–145 (1961).
  113. Grassle, J. F. Deep-sea benthic biodiversity. *BioScience* **41**, 464–469 (1991).
  114. Heiple, Z. et al. Many ways to build an angler: diversity of feeding morphologies in a deep-sea evolutionary radiation. *Biol. Lett.* **19**, 20230049 (2023).
  115. Bertelsen, E. *The Ceratioid Fishes. Ontogeny, Taxonomy, Distribution and Biology* Dana Reports Vol. **39** (Brill, 1951).
  116. Moore, J. A. Upside-down swimming behavior in a whipnose anglerfish (Teleostei: Ceratioidei: Gigantactinidae). *Copeia* **2002**, 1144–1146 (2002).
  117. Stewart, A. L., Pietsch, T. W., Moore, J. & Peng, X. Upside-down swimming: in situ observations of inverted orientation in *Gigantactis*, with a new depth record for the Ceratioidei. *J. Fish. Biol.* **104**, 887–891 (2023).
  118. Draghi, J. A., Ogbunugafor, C. B., Zaman, L. & Parsons, T. Relaxed selection can speed the evolution of complex adaptations. Preprint at bioRxiv <https://doi.org/10.1101/2024.07.09.602773> (2024).
  119. Stroud, J. T., Moore, M. P., Langerhans, R. B. & Losos, J. B. Fluctuating selection maintains distinct species phenotypes in an ecological community in the wild. *Proc. Natl Acad. Sci. USA* **120**, e2222071120 (2023).
  120. Luck, D. G. & Pietsch, T. W. In situ observations of a deep-sea ceratioid anglerfish of the genus *Oneirodes* (Lophiiformes: Oneirodidae). *Copeia* **2008**, 446–451 (2008).
  121. Alfaro, M. E. et al. Explosive diversification of marine fishes at the Cretaceous–Palaeogene boundary. *Nat. Ecol. Evol.* **2**, 688–696 (2018).
  122. Bolger, A. M., Lohse, M. & Usadel, B. Trimmomatic: a flexible trimmer for Illumina sequence data. *Bioinformatics* **30**, 2114–2120 (2014).
  123. Li, H. & Durbin, R. Fast and accurate short read alignment with Burrows–Wheeler transform. *Bioinformatics* **25**, 1754–1760 (2009).
  124. Li, H. et al. The Sequence Alignment/Map format and SAMtools. *Bioinformatics* **25**, 2078–2079 (2009).
  125. Zerbino, D. R. & Birney, E. Velvet: algorithms for de novo short read assembly using de Bruijn graphs. *Genome Res.* **18**, 821–829 (2008).
  126. Allen, J. M. et al. Phylogenomics from whole genome sequences using aTRAM. *Syst. Biol.* **66**, 786–798 (2017).
  127. Grabherr, M. G. et al. Full-length transcriptome assembly from RNA-Seq data without a reference genome. *Nat. Biotechnol.* **29**, 644–652 (2011).
  128. Li, W. & Godzik, A. Cd-hit: a fast program for clustering and comparing large sets of protein or nucleotide sequences. *Bioinformatics* **22**, 1658–1659 (2006).
  129. Fu, L., Niu, B., Zhu, Z., Wu, S. & Li, W. CD-HIT: accelerated for clustering the next-generation sequencing data. *Bioinformatics* **28**, 3150–3152 (2012).
  130. Slater, G. S. C. & Birney, E. Automated generation of heuristics for biological sequence comparison. *BMC Bioinformatics* **6**, 31 (2005).
  131. Ranwez, V., Douzery, E. J. P., Cambon, C., Chantret, N. & Delsuc, F. MACSE v2: toolkit for the alignment of coding sequences accounting for frameshifts and stop codons. *Mol. Biol. Evol.* **35**, 2582–2584 (2018).

132. Arcila, D. et al. Testing the utility of alternative metrics of branch support to address the ancient evolutionary radiation of tunas, stromateoids, and allies (Teleostei: Pelagiaria). *Syst. Biol.* **70**, 1123–1144 (2021).
133. Simion, P. et al. A large and consistent phylogenomic dataset supports sponges as the sister group to all other animals. *Curr. Biol.* **27**, 958–967 (2017).
134. Nguyen, L.-T., Schmidt, H. A., von Haeseler, A. & Minh, B. Q. IQ-TREE: a fast and effective stochastic algorithm for estimating maximum-likelihood phylogenies. *Mol. Biol. Evol.* **32**, 268–274 (2015).
135. Kapli, P., Yang, Z. & Telford, M. J. Phylogenetic tree building in the genomic age. *Nat. Rev. Genet.* **21**, 428–444 (2020).
136. Ratnasingham, S. & Hebert, P. D. N. bold: the Barcode of Life Data System (<http://www.barcodinglife.org>). *Mol. Ecol. Notes* **7**, 355–364 (2007).
137. Lemoine, F. & Gascuel, O. Gotree/Goalign: toolkit and Go API to facilitate the development of phylogenetic workflows. *NAR Genom. Bioinform.* **3**, lqab075 (2021).
138. Borowiec, M. L. AMAS: a fast tool for alignment manipulation and computing of summary statistics. *PeerJ* **4**, e1660 (2016).
139. Hoang, D. T., Chernomor, O., von Haeseler, A., Minh, B. Q. & Vinh, L. S. UFBoot2: improving the ultrafast bootstrap approximation. *Mol. Biol. Evol.* **35**, 518–522 (2018).
140. Mirarab, S. & Warnow, T. ASTRAL-II: coalescent-based species tree estimation with many hundreds of taxa and thousands of genes. *Bioinformatics* **31**, i44–i52 (2015).
141. Zhang, C., Rabiee, M., Sayyari, E. & Mirarab, S. ASTRAL-III: polynomial time species tree reconstruction from partially resolved gene trees. *BMC Bioinformatics* **19**, 15–30 (2018).
142. Sayyari, E. & Mirarab, S. Fast coalescent-based computation of local branch support from quartet frequencies. *Mol. Biol. Evol.* **33**, 1654–1668 (2016).
143. Parham, J. F. et al. Best practices for justifying fossil calibrations. *Syst. Biol.* **61**, 346–359 (2012).
144. Santini, F. & Tyler, J. C. A phylogeny of the families of fossil and extant tetraodontiform fishes (Acanthomorpha, Tetraodontiformes), Upper Cretaceous to Recent. *Zool. J. Linn. Soc.* **139**, 565–617 (2003).
145. Arcila, D., Alexander Pyron, R., Tyler, J. C., Ortí, G. & Betancur-R., R. An evaluation of fossil tip-dating versus node-age calibrations in tetraodontiform fishes (Teleostei: Percomorphaceae). *Mol. Phylogenet. Evol.* **82**, 131–145 (2015).
146. Friedman, M. et al. Molecular and fossil evidence place the origin of cichlid fishes long after Gondwanan rifting. *Proc. R. Soc. B* **280**, 20131733 (2013).
147. Santini, F., Sorenson, L. & Alfaro, M. E. A new phylogeny of tetraodontiform fishes (Tetraodontiformes, Acanthomorpha) based on 22 loci. *Mol. Phylogenet. Evol.* **69**, 177–187 (2013).
148. Dornburg, A., Townsend, J. P., Friedman, M. & Near, T. J. Phylogenetic informativeness reconciles ray-finned fish molecular divergence times. *BMC Evol. Biol.* **14**, 169 (2014).
149. Mello, B., Tao, Q., Barba-Montoya, J. & Kumar, S. Molecular dating for phylogenies containing a mix of populations and species by using Bayesian and RelTime approaches. *Mol. Ecol. Resour.* **21**, 122–136 (2021).
150. Costa, F. P., Schrago, C. G. & Mello, B. Assessing the relative performance of fast molecular dating methods for phylogenomic data. *BMC Genomics* **23**, 798 (2022).
151. Hedman, M. M. Constraints on clade ages from fossil outgroups. *Paleobiology* **36**, 16–31 (2010).
152. Yang, Z. PAML 4: Phylogenetic Analysis by Maximum Likelihood. *Mol. Biol. Evol.* **24**, 1586–1591 (2007).
153. Rambaut, A., Drummond, A. J., Xie, D., Baele, G. & Suchard, M. A. Posterior summarization in Bayesian phylogenetics using Tracer 1.7. *Syst. Biol.* **67**, 901–904 (2018).
154. Stecher, G., Tamura, K. & Kumar, S. Molecular Evolutionary Genetics Analysis (MEGA) for macOS. *Mol. Biol. Evol.* **37**, 1237–1239 (2020).
155. Matzke, N. J. Model selection in historical biogeography reveals that founder-event speciation is a crucial process in island clades. *Syst. Biol.* **63**, 951–970 (2014).
156. Froese, R. & Pauly, D. (eds) *FishBase* (FishBase, 2023); <https://www.fishbase.org/>
157. *Fishes of Australia* (Museums Victoria, 2018); <http://fishesofaustralia.net.au/>
158. Burnham, K. P. & Anderson, D. R. *Model Selection and Multimodel Inference: A Practical Information-Theoretic Approach* (Springer, 2002).
159. Ree, R. H. & Smith, S. A. Maximum likelihood inference of geographic range evolution by dispersal, local extinction, and cladogenesis. *Syst. Biol.* **57**, 4–14 (2008).
160. Ronquist, F. Dispersal-vicariance analysis: a new approach to the quantification of historical biogeography. *Syst. Biol.* **46**, 195–203 (1997).
161. Landis, M. J., Matzke, N. J., Moore, B. R. & Huelsenbeck, J. P. Bayesian analysis of biogeography when the number of areas is large. *Syst. Biol.* **62**, 789–804 (2013).
162. Beaulieu, J. M. & O'Meara, B. C. Detecting hidden diversification shifts in models of trait-dependent speciation and extinction. *Syst. Biol.* **65**, 583–601 (2016).
163. Nakov, T. gghisse. GitHub <https://github.com/discindo/gghisse> (2023).
164. Louca, S. & Pennell, M. W. Extant timetrees are consistent with a myriad of diversification histories. *Nature* **580**, 502–505 (2020).
165. O'Meara, B. & Beaulieu, J. M. Potential survival of some, but not all, diversification methods. Preprint at <https://ecoenvorxiv.org/repository/view/3912/> (2021).
166. Claude, J. Log-shape ratios, procrustes superimposition, elliptic Fourier analysis: three worked examples in R. *Hystrix It. J. Mammal.* **24**, 94–102 (2013).
167. Baken, E. K., Collyer, M. L., Kaliontzopoulou, A. & Adams, D. C. geomorph v4.0 and gmShiny: enhanced analytics and a new graphical interface for a comprehensive morphometric experience. *Methods Ecol. Evol.* **12**, 2355–2363 (2021).
168. Hothorn, T., Bretz, F. & Westfall, P. Simultaneous inference in general parametric models. *Biom. J.* **50**, 346–363 (2008).
169. Buser, T. J. et al. The natural historian's guide to the CT Galaxy: step-by-step instructions for preparing and analyzing computed tomographic (CT) data using cross-platform, open access software. *Integr. Org. Biol.* **2**, obaa009 (2020).
170. Amira v.2020.3 (Thermo Fisher Scientific, 2020).
171. Stratovan Checkpoint version 2020.10.13.0859 (Stratovan Corporation, 2020).
172. Mardia, K. V., Bookstein, F. L. & Moreton, I. J. Statistical assessment of bilateral symmetry of shapes. *Biometrika* **92**, 249–250 (2005).
173. Westneat, M. W. Evolution of levers and linkages in the feeding mechanisms of fishes. *Integr. Comp. Biol.* **44**, 378–389 (2004).
174. Vidal-García, M., Bandara, L. & Keogh, J. S. ShapeRotator: an R tool for standardized rigid rotations of articulated three-dimensional structures with application for geometric morphometrics. *Ecol. Evol.* **8**, 4669–4675 (2018).
175. Rhoda, D., Segall, M., Larouche, O., Evans, K. & Angielczyk, K. D. Local superimpositions facilitate morphometric analysis of complex articulating structures. *Integr. Comp. Biol.* **61**, 1892–1904 (2021).
176. Sidlauskas, B. Continuous and arrested morphological diversification in sister clades of characiform fishes: a phylomorphospace approach. *Evolution* **62**, 3135–3156 (2008).
177. Goswami, A. & Clavel, J. Morphological evolution in a time of phenomics. Preprint at <https://ecoenvorxiv.org/repository/view/6507/> (2024).

178. Adams, D. C. & Collyer, M. L. Multivariate phylogenetic comparative methods: evaluations, comparisons, and recommendations. *Syst. Biol.* **67**, 14–31 (2018).
179. Clavel, J., Aristide, L. & Morlon, H. A penalized likelihood framework for high-dimensional phylogenetic comparative methods and an application to new-world monkeys brain evolution. *Syst. Biol.* **68**, 93–116 (2019).
180. Blackburn, D. C. et al. Increasing the impact of vertebrate scientific collections through 3D imaging: the openVertebrate (oVert) Thematic Collections Network. *BioScience* **74**, 169–186 (2024).
181. Felice, R. N., Pol, D. & Goswami, A. Complex macroevolutionary dynamics underly the evolution of the crocodyliform skull. *Proc. R. Soc. B.* **288**, 20210919 (2021).
182. Butler, M. A. & King, A. A. Phylogenetic comparative analysis: a modeling approach for adaptive evolution. *Am. Nat.* **164**, 683–695 (2004).
183. Grabowski, M. et al. A cautionary note on “A cautionary note on the use of Ornstein Uhlenbeck models in macroevolutionary studies”. *Syst. Biol.* **72**, 955–963 (2023).
184. Beaulieu, J. M., Jhuang, D.-C., Boettiger, C. & O’Meara, B. C. Modeling stabilizing selection: expanding the Ornstein-Uhlenbeck model of adaptive evolution. *Evolution* **66**, 2369–2383 (2012).
185. Beaulieu, J. M. & O’Meara, B. C. OUwie: Analysis of Evolutionary Rates in an OU Framework (CRAN, 2016); <https://cran.r-project.org/web/packages/OUwie/OUwie.pdf>
186. Plummer, M., Best, N. & Cowles, K. CODA: convergence diagnosis and output analysis for MCMC. *R News* **6**, 7–11 (2006).
187. Ferguson-Gow, H. BTprocessR: a set of tools to help with the interpretation and analysis of the output of BayesTraits MCMC analyses. *GitHub* <https://rdrr.io/github/hferg/BTprocessR/> (2020).
188. Ferguson-Gow, H. btrtools: a set of tools for processing and analysing the output of BayesTraits. *GitHub* <https://rdrr.io/github/hferg/btrtools/> (2017).
189. Hughes, L. Tutorial for assembling exon capture data across the diversity of fishes. *GitHub* <https://github.com/lilychughes/FishLifeExonCapture> (2021).
190. Carpenter, K. E. & Niem, V. H. (eds) *The Living Marine Resources of the Western Central Pacific* Vol. 3 (FAO, 1999).

## Acknowledgements

We thank the following museums and personnel for providing voucher specimens and/or tissues: UWFC (K. Maslenikov), FLMNH (R. Robins), SIO (B. Frable and P. Hastings), AM (A. Hay), CSIRO (A. Graham and J. Pogonoski), MCZ (A. Williston and M. Sorce), FSBC (E. Post), YPM (G. Watkins-Colwell and T. Near), KU (A. Bentley and L. Smith), LSUMZ (P. Chakrabarty and S. Parker), LACM (T. Clardy and B. Ludt) and USNM (C. Huddleston and D. Pitassy). T. Sutton kindly gifted tissues to UWFC. We thank A. Summers, K. Cohen and Z. Heiple for help with µCT scanning at Friday Harbor Laboratories. Scanning was supported by the oVert TCN (NSF DBI-1701665). S. Panciroli, D. Patterson, L. MacLeod, J. Huie and J. Gardner assisted with collecting and processing µCT scans and were funded by the William W. and Dorothy T. Gilbert

Ichthyology Research Fund. T. Buser, S. Friedman, O. Larouche, E. Troyer, J. Clavel and A. Meade gave advice on morphometric approaches and comparative methods. We thank the MERLAB at the University of Washington for assistance with wet lab work. Exon capture and sequencing was performed by Arbor Biosciences and partially funded by FishLife (NSF DEB-1541554 and NSF DEB-2144325). Computational resources were provided by the University of Oklahoma Supercomputing Center for Education and Research (OSCER). L. Ward assisted with data curation and quality control. Additional funding was provided by NSF Postdoctoral Fellowships (DBI-1906574 to E.C.M. and DBI-2109469 to P.B.H.); NSF DEB-2237278 to K.E.; NSF DEB-2144325 and NSF DEB-2015404 to D.A.

## Author contributions

E.C.M., L.T. and D.A. conceptualized the study. E.C.M., P.B.H. and M.R.-S. collected and curated molecular data. E.C.M. and A.S. curated fossil information and oversaw time calibration. W.T.W., C.C.B. and M.M. contributed anglerfish tissues. E.C.M. and R.F. collected and processed µCT scans and body shape data. E.C.M. and K.E. designed and performed comparative analyses. E.C.M. and R.F. jointly led the project. L.T., K.E., R.B.-R. and D.A. jointly supervised the project.

## Competing interests

The authors declare no competing interests.

## Additional information

**Extended data** is available for this paper at <https://doi.org/10.1038/s41559-024-02586-3>.

**Supplementary information** The online version contains supplementary material available at <https://doi.org/10.1038/s41559-024-02586-3>.

**Correspondence and requests for materials** should be addressed to Elizabeth Christina Miller.

**Peer review information** *Nature Ecology & Evolution* thanks Laura Wilson and the other, anonymous, reviewer(s) for their contribution to the peer review of this work.

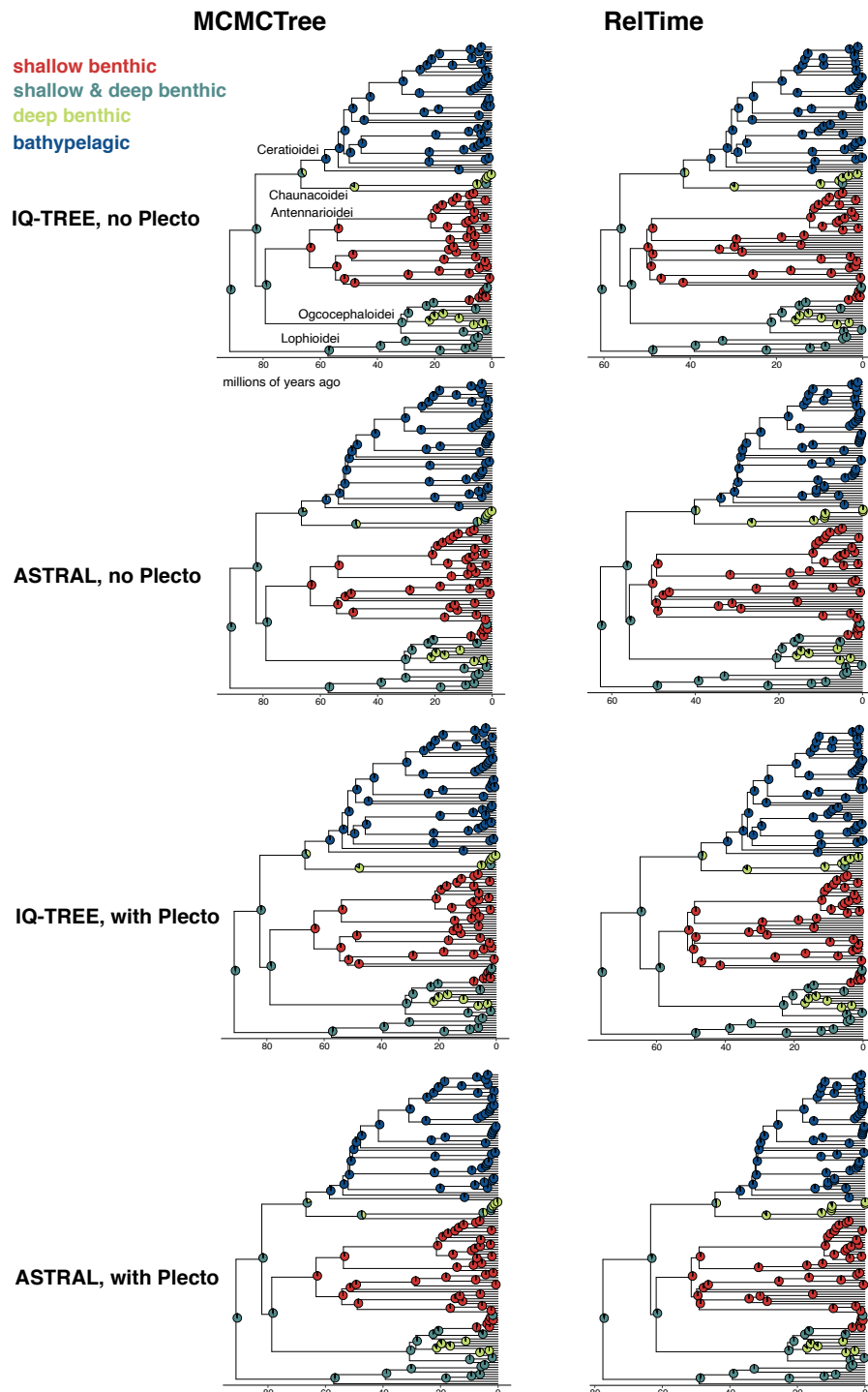
**Reprints and permissions information** is available at [www.nature.com/reprints](http://www.nature.com/reprints).

**Publisher’s note** Springer Nature remains neutral with regard to jurisdictional claims in published maps and institutional affiliations.

Springer Nature or its licensor (e.g. a society or other partner) holds exclusive rights to this article under a publishing agreement with the author(s) or other rightsholder(s); author self-archiving of the accepted manuscript version of this article is solely governed by the terms of such publishing agreement and applicable law.

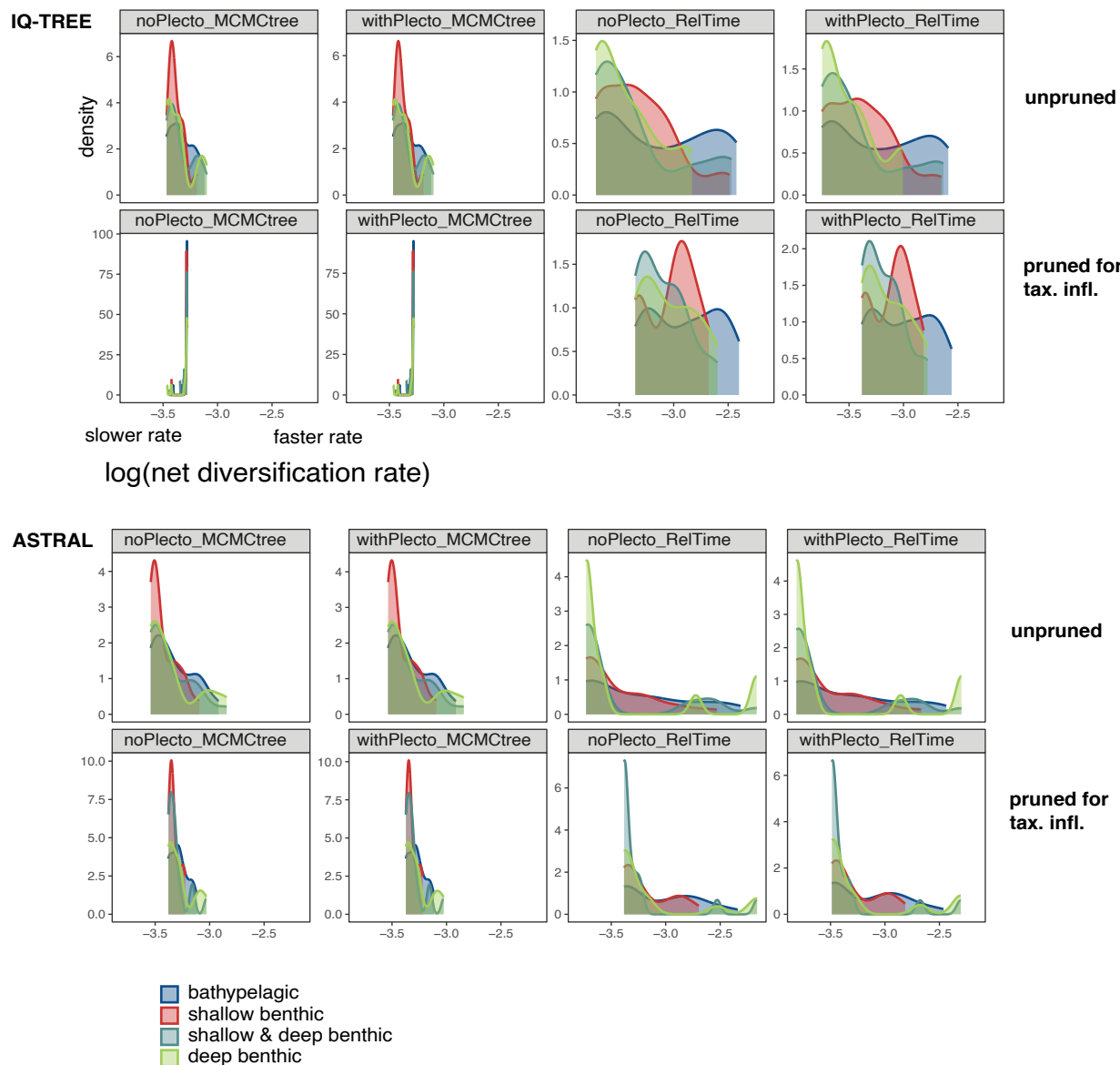
© The Author(s), under exclusive licence to Springer Nature Limited 2024

<sup>1</sup>Department of Biology, University of Oklahoma, Norman, OK, USA. <sup>2</sup>Department of Ichthyology, Sam Noble Museum of Natural History, Norman, OK, USA. <sup>3</sup>School of Aquatic and Fishery Sciences, University of Washington, Seattle, WA, USA. <sup>4</sup>Burke Museum of Natural History and Culture, University of Washington, Seattle, WA, USA. <sup>5</sup>Marine Biology Research Division, Scripps Institution of Oceanography, University of California San Diego, La Jolla, CA, USA. <sup>6</sup>Department of Biosciences, Rice University, Houston, TX, USA. <sup>7</sup>Department of Biological Sciences, University of Alabama, Tuscaloosa, AL, USA. <sup>8</sup>CSIRO Australian National Fish Collection, National Research Collections Australia, Hobart, Tasmania, Australia. <sup>9</sup>Department of Vertebrate Zoology, National Museum of Natural History, Smithsonian Institution, Washington, DC, USA. <sup>10</sup>Department of Zoology, Natural History Museum and Institute, Chuo-ku, Chiba, Japan. <sup>11</sup>These authors contributed equally: Elizabeth Christina Miller, Rose Faucher. ✉ e-mail: liz.miller@uci.edu

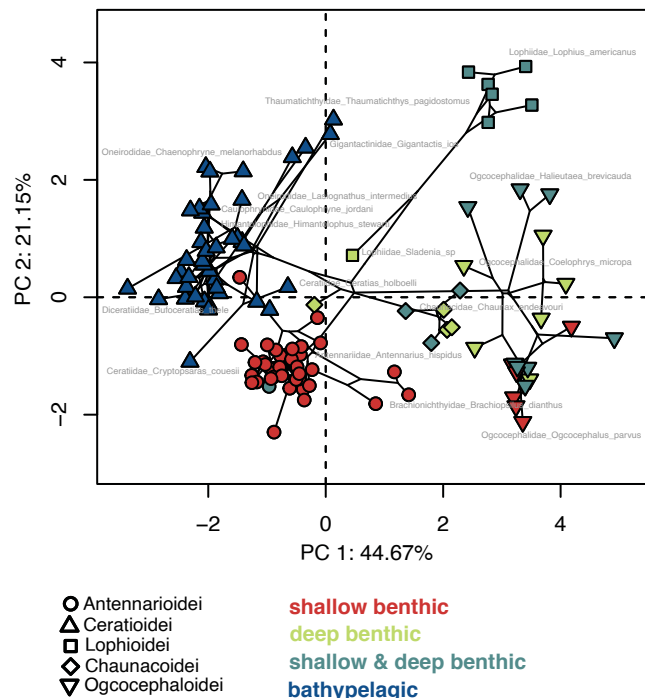
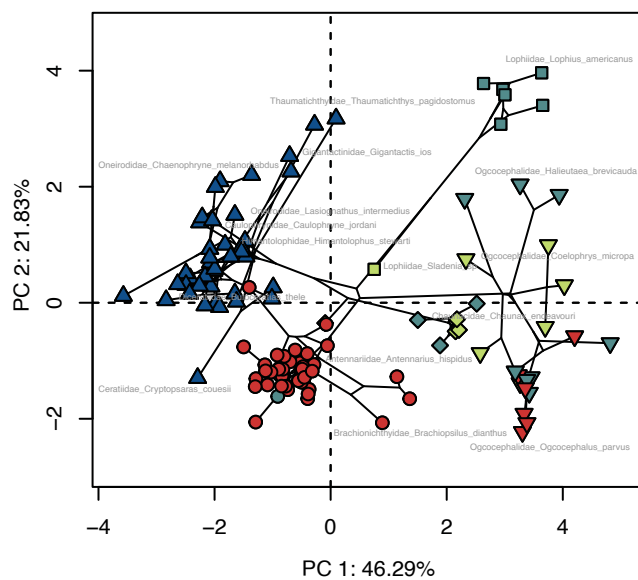


**Extended Data Fig. 1 | Ancestral habitats for anglerfishes.** BioGeoBEARS results are shown for all eight input trees. For BioGeoBEARS model fits see Supplementary Table 5.

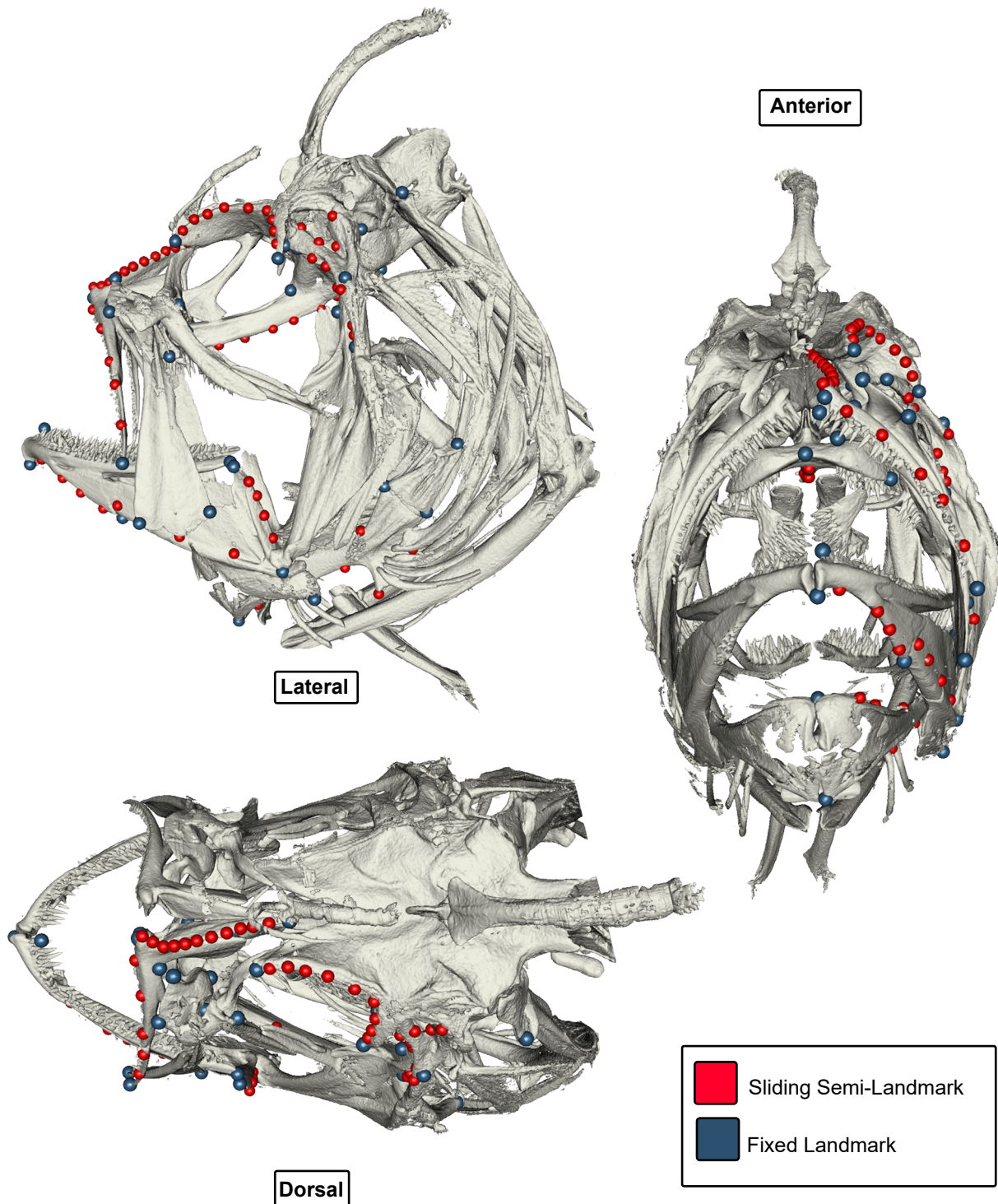
## MiSSE tip rates by habitat



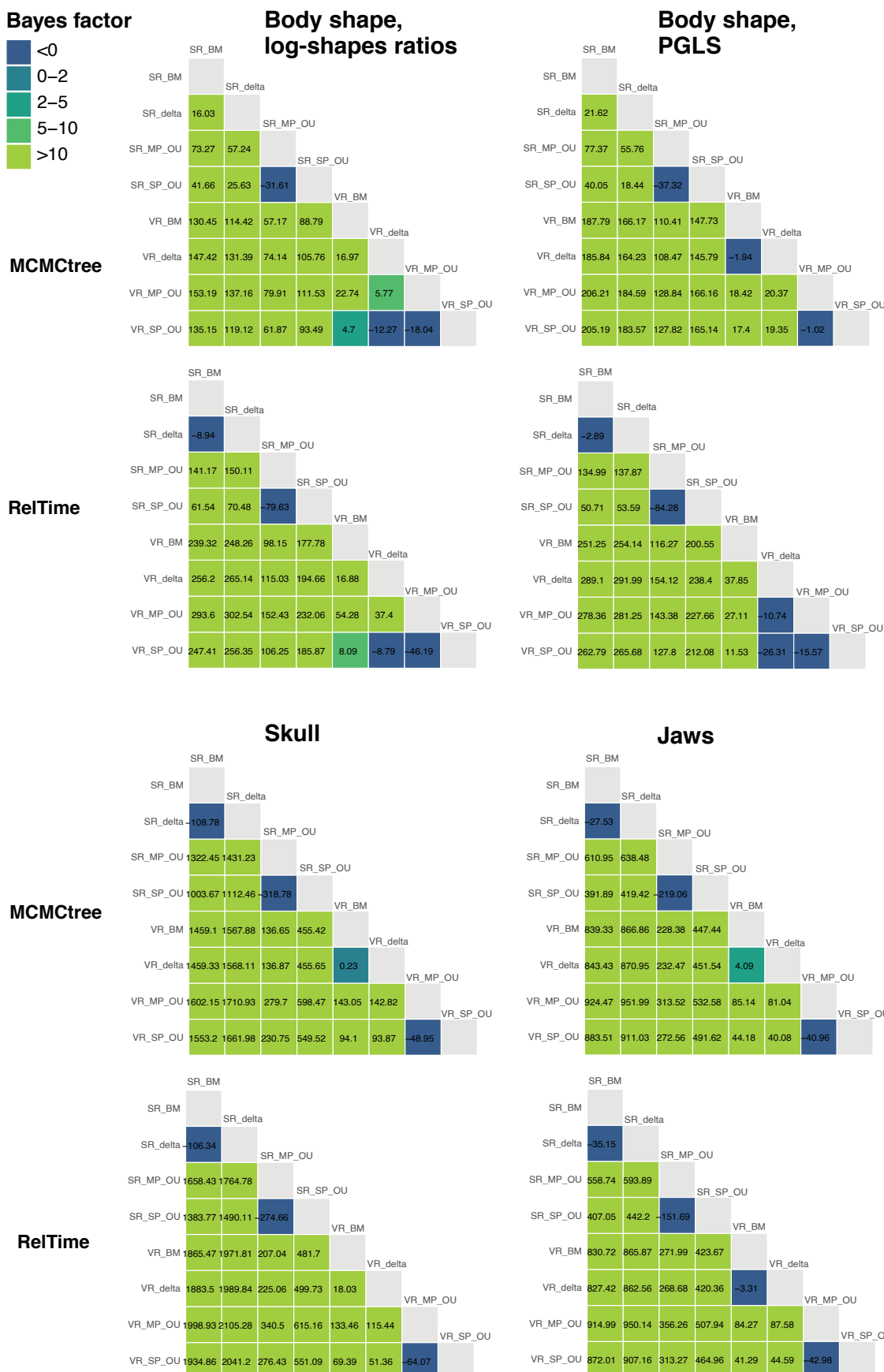
**Extended Data Fig. 2 | Recent lineage diversification rates by habitat.** Model-averaged tip rates estimated by MiSSE. For MiSSE model fits see Supplementary Table 6. Pruning *Himantolophus* and *Ogcocephalus* to adjust for suspected taxonomic inflation (Appendix A2) had little influence on the results other than reducing overall rate variation.

**A) Body shape, log-shape ratios****B) Body shape, PGLS residuals**

**Extended Data Fig. 3 | Allometry had little influence on overall morphological diversity.** Phylomorphospace of body shape with linear measurements size-corrected using (A) log-shape ratios or (B) PGLS residuals, the latter of which removes effects of allometry on shape. Taxa are colored by habitat and shaped by clade. Select taxa are noted.



**Extended Data Fig. 4** | Illustration of landmarks placed on  $\mu$ CT scans for geometric morphometrics.

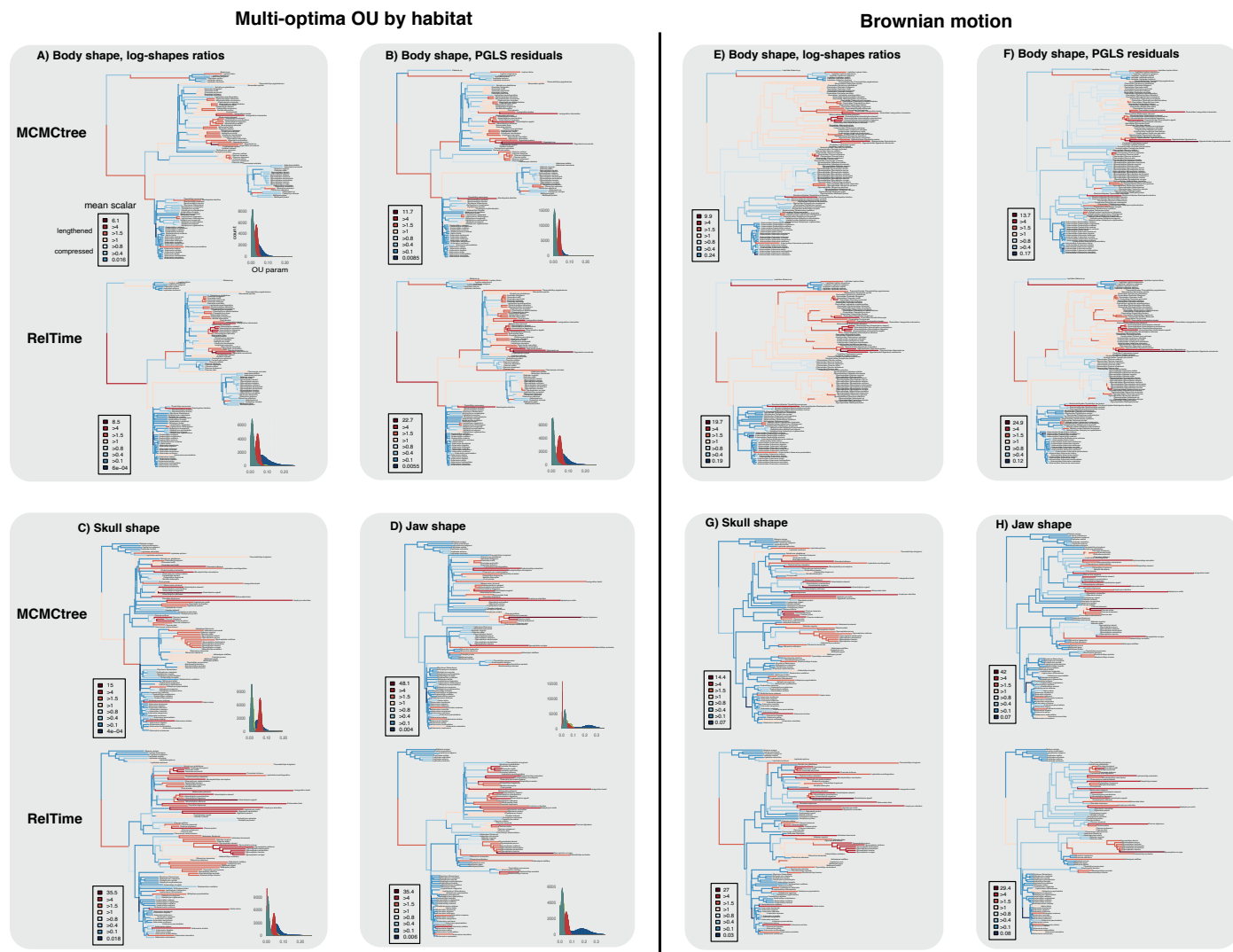


**Extended Data Fig. 5 | See next page for caption.**

**Extended Data Fig. 5 | BayesTraits model comparison with Bayes Factors.**

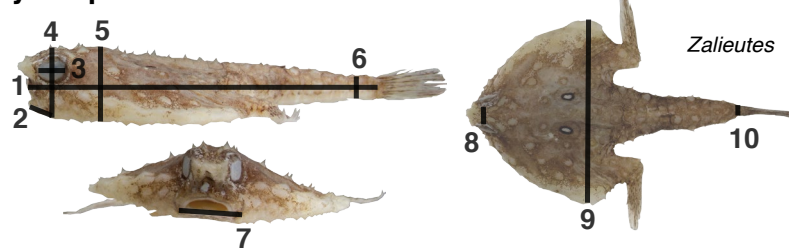
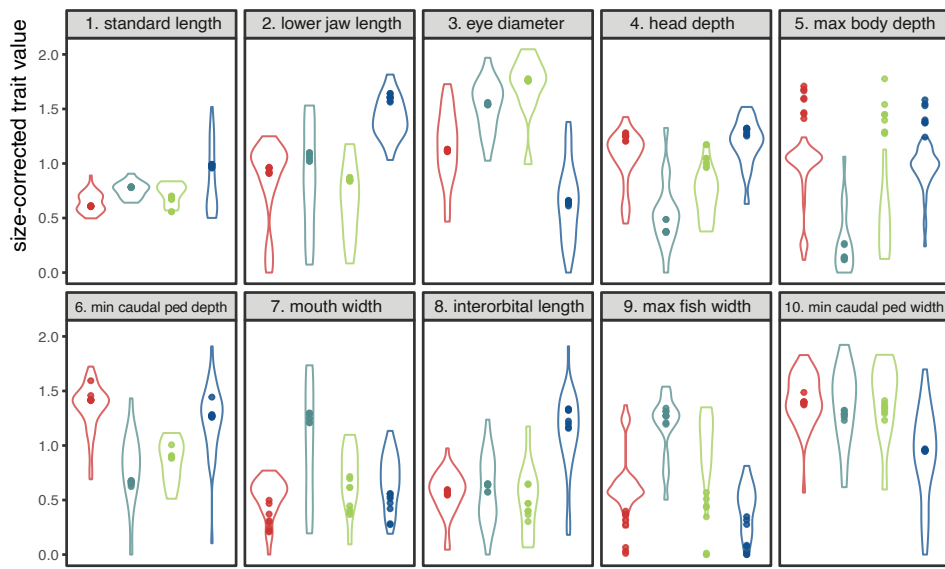
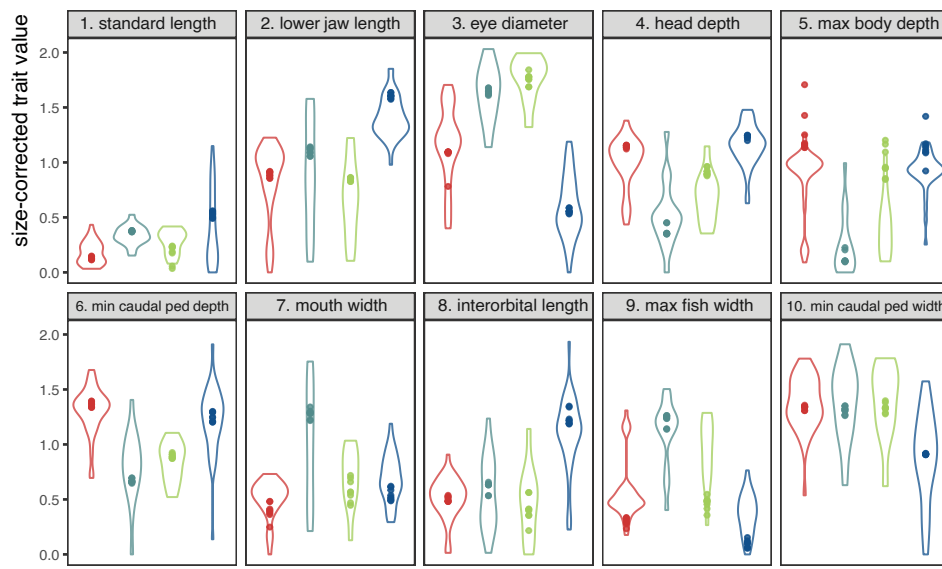
Models are fit using transformations of the input tree consistent with predictions of different evolutionary scenarios. SR\_BM = single-rate Brownian motion; SR\_delta = single-rate early burst; SR\_MP\_OU = single-rate multiple-peak Ornstein–Uhlenbeck

by habitat; SR\_SP\_OU = single-rate single-peak OU; VR\_BM = variable-rate Brownian motion; VR\_delta = variable-rate early burst; VR\_MP\_OU = variable-rate multiple-peak OU by habitat; VR\_SP\_OU = variable-rate single-peak OU.



**Extended Data Fig. 6 | Comparing BayesTraits results across trees, datasets, and models.** Branch lengths are scaled according to morphological change. For multi-optima OU models, scalars reflect both the OU parameter (strength of selection; shown in grey panel) and evolutionary rate; for Brownian motion models branch lengths are scaled based on the evolutionary rate only. Warm

colors and scalars > 1 indicate that branch length was increased; cool colors and scalars < 1 indicate that the branch length was compressed. Results are compared using a tree calibrated with MCMCTree versus RelTime, and with size-correction approaches that preserve or remove effects of allometry.

**A) Body shape variables****B) OUwie trait optima, using log-shape ratios****C) OUwie trait optima, using PGLS residuals**

- shallow benthic
- shallow & deep benthic
- deep benthic
- bathypelagic

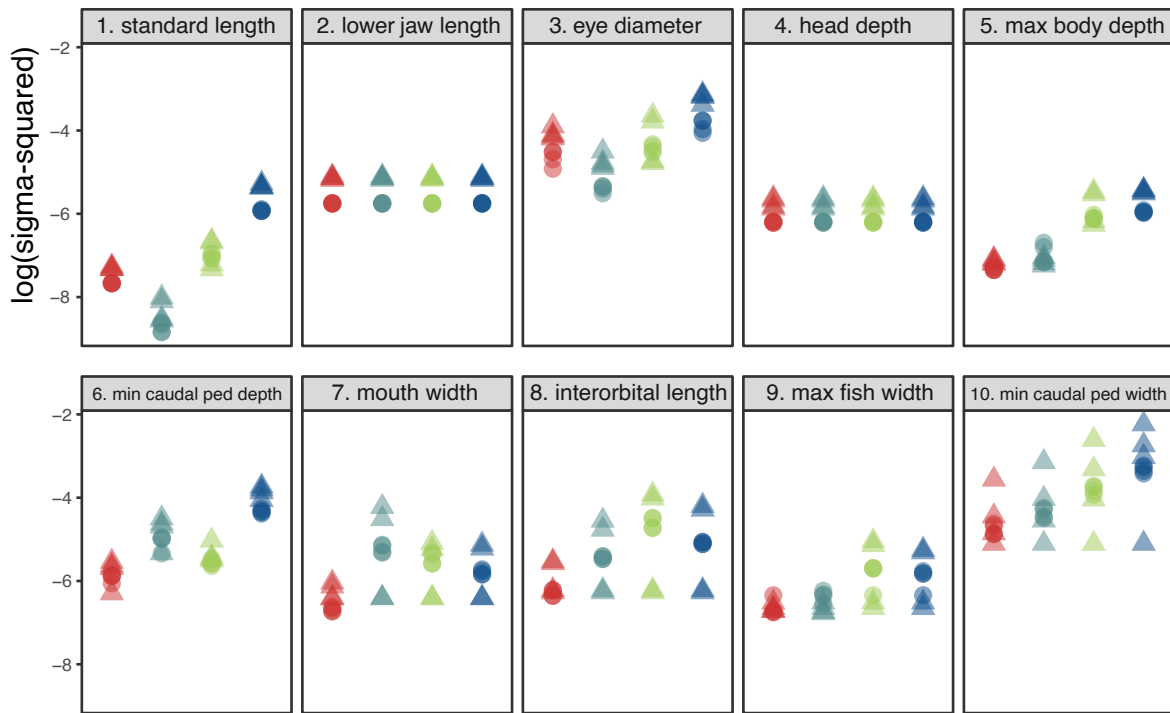
Extended Data Fig. 7 | See next page for caption.

**Extended Data Fig. 7 | Habitat optima for individual body shape variables.**

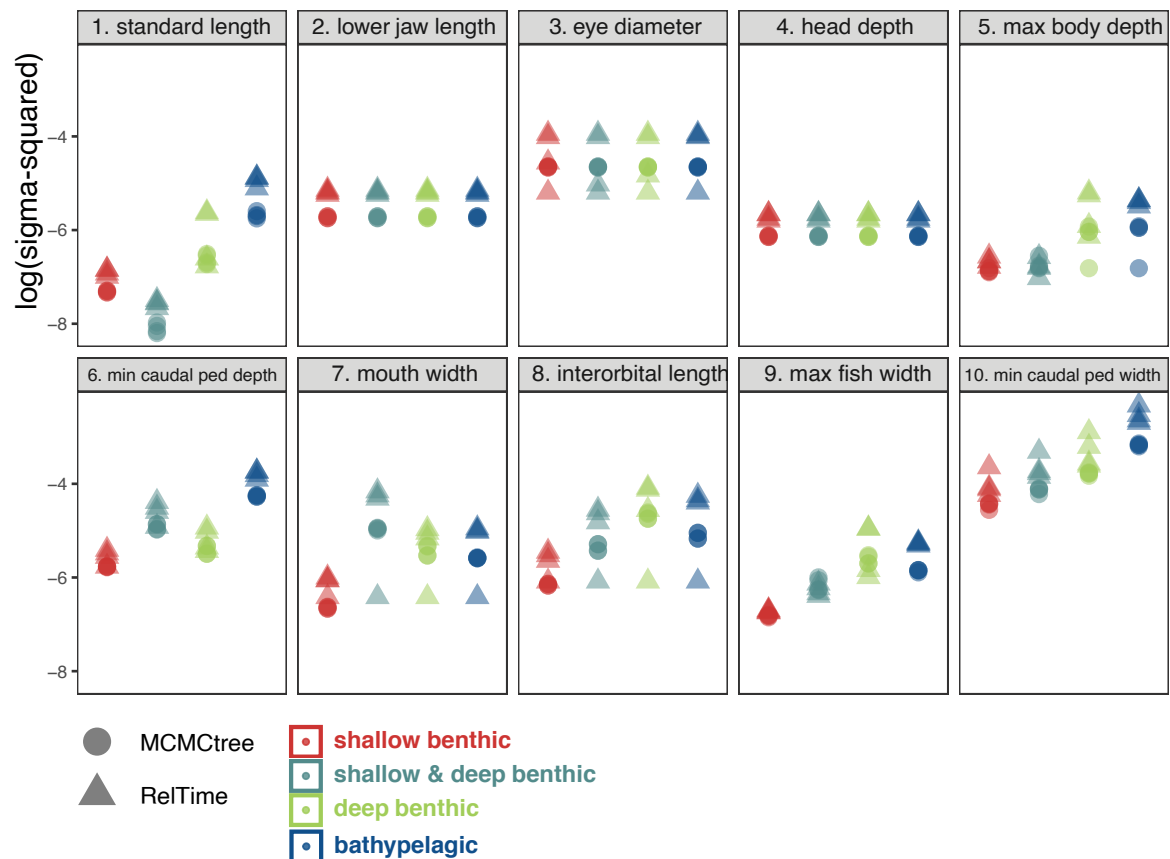
(A) Illustration of the ten linear measurements taken to approximate overall body shape. (B–C) Variation in trait values are shown by violin plots, after size-correction with (B) log-shape ratios or (C) PGLS residuals (removing effects

of allometry). Circles represent the OU optimum inferred by the best-fitting OUwie model using each of the eight input trees. For OUwie model fits see Supplementary Table 8.

### A) OUwie evolutionary rates, using log-shape ratios

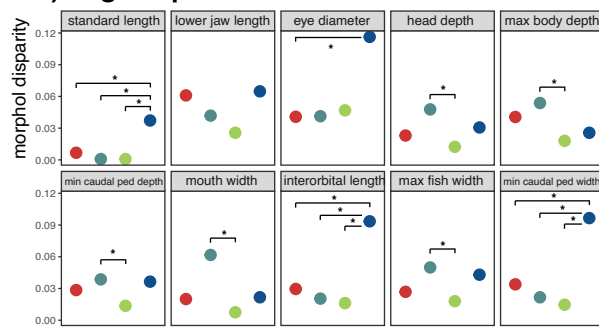
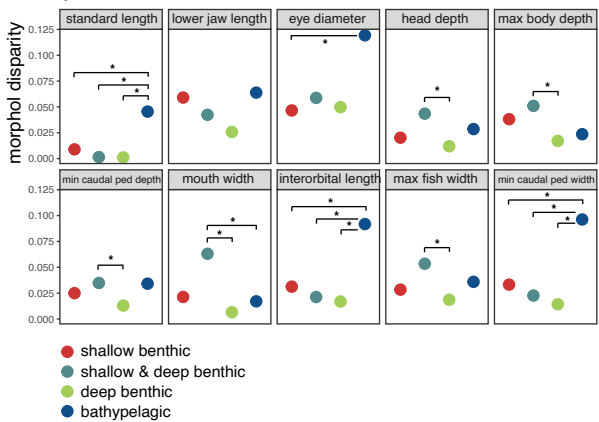


### B) OUwie evolutionary rates, using PGLS residuals



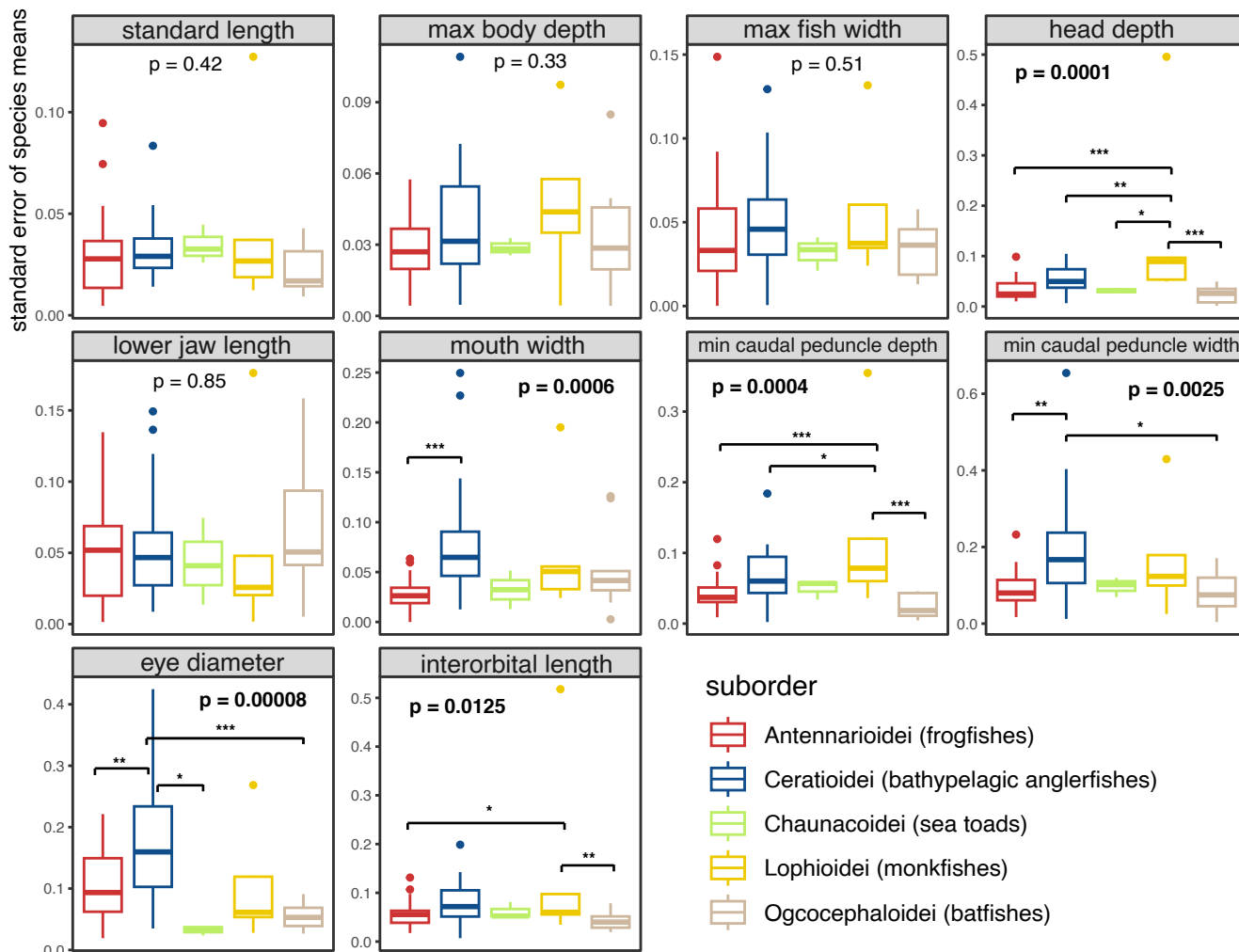
Extended Data Fig. 8 | See next page for caption.

**Extended Data Fig. 8 | Evolutionary rates for individual body shape variables by habitat.** Rates inferred under best-fitting OUwie models across eight alternative input trees are shown. Variables were size corrected using log-shape ratios (**A**) or PGLS residuals (**B**), the latter of which removes effects of allometry. For OUwie model fits see Supplementary Table 8.

**A) Log-shape ratios****B) PGLS residuals**

**Extended Data Fig. 9 | Disparity in individual body shape variables by habitat.** Variables were size corrected using log-shape ratios (A) or PGLS residuals (B), the latter of which removes effects of allometry. Significant pairwise comparisons are noted with “\*”. For full disparity results see Appendix 5 in ref. 77.

## Standard error by trait



**Extended Data Fig. 10 | Measurement error by clade.** Standard error of species means (calculated from 70 species for which >1 individuals were measured) is shown for ten linear body shape measurements (illustrated in Extended Data Fig. 7). Standard errors were compared statistically using a one-way ANOVA with

a post-hoc Tukey test of pairwise comparisons (\* indicates  $p < 0.05$ ; \*\* indicates  $p < 0.01$ ; \*\*\* indicates  $p < 0.001$ ). Standard errors were inputted during OUwie model fitting to account for measurement error and specimen deformation.

## Reporting Summary

Nature Portfolio wishes to improve the reproducibility of the work that we publish. This form provides structure for consistency and transparency in reporting. For further information on Nature Portfolio policies, see our [Editorial Policies](#) and the [Editorial Policy Checklist](#).

### Statistics

For all statistical analyses, confirm that the following items are present in the figure legend, table legend, main text, or Methods section.

n/a Confirmed

- The exact sample size ( $n$ ) for each experimental group/condition, given as a discrete number and unit of measurement
- A statement on whether measurements were taken from distinct samples or whether the same sample was measured repeatedly
- The statistical test(s) used AND whether they are one- or two-sided  
*Only common tests should be described solely by name; describe more complex techniques in the Methods section.*
- A description of all covariates tested
- A description of any assumptions or corrections, such as tests of normality and adjustment for multiple comparisons
- A full description of the statistical parameters including central tendency (e.g. means) or other basic estimates (e.g. regression coefficient) AND variation (e.g. standard deviation) or associated estimates of uncertainty (e.g. confidence intervals)
- For null hypothesis testing, the test statistic (e.g.  $F$ ,  $t$ ,  $r$ ) with confidence intervals, effect sizes, degrees of freedom and  $P$  value noted  
*Give  $P$  values as exact values whenever suitable.*
- For Bayesian analysis, information on the choice of priors and Markov chain Monte Carlo settings
- For hierarchical and complex designs, identification of the appropriate level for tests and full reporting of outcomes
- Estimates of effect sizes (e.g. Cohen's  $d$ , Pearson's  $r$ ), indicating how they were calculated

*Our web collection on [statistics for biologists](#) contains articles on many of the points above.*

### Software and code

Policy information about [availability of computer code](#)

## Data collection

Pipelines for assembly of newly collected exon-capture data are public: <https://github.com/lilychughes/FishLifeExonCapture>

This same pipeline can be used to mine exons from other types of data such as UCEs.

## Data analysis

R scripts and inputs needed to replicate analyses are available in a Dryad repository (doi: <https://doi.org/10.5061/dryad.n2z34tn5r>).

The following public open source programs were used for analyses:

## Genomic assembly:

Trimmomatic v.0.39; BWA v.0.7.17; SAMtools v.1.9; Velvet v.1.2.10; aTRAM 2.2; Trinity v.2.2; CD-HIT-EST v.4.8.1; Exonerate v.2.4.0; MACSE v.2.03

## Phylogenomic inference:

AMAS; IQ-TREE MPI multicore v.2.0; ASTRAL-II v.5.7.1

## Divergence time estimation:

PAML v.4.9h; MEGAX

## Phylogenetic comparative methods:

BioGeoBEARS v.1.1.3; hisse v2.1.1; geomorph v.4.0.5; geiger v.2.0.11; BayesTraits V4; OUwie v.2.10

The BayesTraits executable can be downloaded here: <https://www.evolution.reading.ac.uk/BayesTraitsV4.0.1/BayesTraitsV4.0.1.html>

For manuscripts utilizing custom algorithms or software that are central to the research but not yet described in published literature, software must be made available to editors and reviewers. We strongly encourage code deposition in a community repository (e.g. GitHub). See the Nature Portfolio [guidelines for submitting code & software](#) for further information.

## Data

Policy information about [availability of data](#)

All manuscripts must include a [data availability statement](#). This statement should provide the following information, where applicable:

- Accession codes, unique identifiers, or web links for publicly available datasets
- A description of any restrictions on data availability
- For clinical datasets or third party data, please ensure that the statement adheres to our [policy](#)

### Data availability:

Raw sequence reads have been archived in National Center for Biotechnology Information (NCBI) Sequence Read Archive with the BioProject number PRJNA1074427. Any pre-existing sequence data used is given in Supplementary Tables S2 and S3 with accession codes. Aligned molecular data are available in the Dryad repository (<https://doi.org/10.5061/dryad.n2z34tn5r>). Phylogenograms, time-calibrated phylogenies and body shape dataset are available in the Dryad repository. All CT scans are publicly available on Morphosource (<https://www.morphosource.org/>) with media numbers in Supplementary Table S7.

### Code availability:

Pipelines for genomic assembly are publically available: <https://github.com/lilychughes/FishLifeExonCapture>. R scripts used to analyze data are available in a Dryad repository (doi: <https://doi.org/10.5061/dryad.n2z34tn5r>).

## Research involving human participants, their data, or biological material

Policy information about studies with [human participants or human data](#). See also policy information about [sex, gender \(identity/presentation\), and sexual orientation](#) and [race, ethnicity and racism](#).

Reporting on sex and gender

NA

Reporting on race, ethnicity, or other socially relevant groupings

NA

Population characteristics

NA

Recruitment

NA

Ethics oversight

NA

Note that full information on the approval of the study protocol must also be provided in the manuscript.

## Field-specific reporting

Please select the one below that is the best fit for your research. If you are not sure, read the appropriate sections before making your selection.

Life sciences       Behavioural & social sciences       Ecological, evolutionary & environmental sciences

For a reference copy of the document with all sections, see [nature.com/documents/nr-reporting-summary-flat.pdf](https://nature.com/documents/nr-reporting-summary-flat.pdf)

## Ecological, evolutionary & environmental sciences study design

All studies must disclose on these points even when the disclosure is negative.

Study description

This study includes a phylogenomic analysis of the order Lophiiformes (anglerfishes). The phylogeny is time-calibrated using information from the fossil record (all fossil information is from published studies). Using these phylogenies, we performed phylogenetic comparative methods to infer the tempo and mode of evolution in this group.

Research sample

Phylogenomic data:

New data was collected from 152 individuals from 120 species of Lophiiformes. Target capture probes were based on a set of 1,105 single-copy nuclear exon markers designed for fish phylogenomics, plus an additional 19 nuclear legacy markers and mitochondrial DNA. Outgroup sampling included one holocentrid (representing the sister lineage to Percomorpha), one ophidid (the earliest diverging member of Percomorpha), one pelagician, two syngnatharians, 18 tetraodontiforms and 15 additional eupercarians. Additionally, we successfully mined 5–357 exons for 93 individuals representing 48 species from published UCE data. An additional 1–5 legacy markers were downloaded from NCBI for 10 species. Our final taxonomic sampling when combining all data and remaining after all quality control steps was 132 ingroup species (37.8% of species and 78.1% of genera in Lophiiformes) and 20 of 21 families (all but the monotypic Lophichthyidae). Suborder-level sampling is as follows: 9 species of Lophioidei (32.1% of species and all four genera), 21 species of Ogocephaloidei (28.7% of species and eight of ten genera), 40 species of Antennarioidei (62.5% of species

and 77.3% of genera [17 of 22 genera]), eight species of Chaunacoidei (50% of species and both genera), and 54 species of Ceratioidei (32.1% of species and 74.3% of genera [26 of 35 ceratioid genera]).

#### Phenotypic data:

Ten linear body shape measurements were taken from 331 individuals representing 113 species (after quality control). Our CT scan dataset contained 100 species of Lophiiformes (n=1 scan per species). Of these, 38 are new to this study, 33 were recently published in another study by the lead author, and 29 were downloaded from the online repositories MorphoSource (<https://www.morphosource.org/>) or Virtual Natural History Museum (<http://vnhm.de/VNHM/index.php>).

#### Sampling strategy

Sequence data from 1-3 individuals per species was collected depending on tissue availability and costs. CT scans were collected for one representative individual per species. Body shape measurements were collected from 1-9 individuals per species. All major lophiiform lineages (suborders and all but one family) were sampled for phylogenetic analysis. As many genera and species were sampled as possible given tissue availability. Outgroups were sampled to cover major acanthomorph lineages following Betancur-R et al. 2017.

#### Data collection

DNA was extracted from tissue samples and quantified by Elizabeth Miller in the MERLAB of the University of Washington (P.I. Luke Tornabene). New DNA sequencing was performed by Arbor Biosciences using FishLife target capture protocols (<https://www.fishtree.org/>). CT scans were obtained at the Karel F. Liem Bio-Imaging Center at the University of Washington Friday Harbor Laboratories as well as Rice University (P.I. Kory Evans). Body shape measurements were collected from museum specimens using calipers by Elizabeth Miller.

#### Timing and spatial scale

Data were collected between 2020–2022 as part of an NSF Postdoctoral Fellowship to Elizabeth Miller.

#### Data exclusions

For divergence time estimation and phylogenetic comparative methods, phylogenies were pruned to one representative individual per species as appropriate for these methods. Phylogenies including all individuals with genetic data can be viewed in the Supplementary Material (Appendix A1).

#### Reproducibility

Multiple individuals per species were included in phylogenetic inference to help confirm species identity. The all-individuals tree is available in Appendix A1. For body shape measurements, 1-9 individuals per species were measured to account for intraspecific variation. R code and inputs needed to replicate analyses can be found in the Dryad repository associated with this study.

#### Randomization

This is not relevant to our study.

#### Blinding

This is not relevant to our study.

Did the study involve field work?  Yes  No

## Reporting for specific materials, systems and methods

We require information from authors about some types of materials, experimental systems and methods used in many studies. Here, indicate whether each material, system or method listed is relevant to your study. If you are not sure if a list item applies to your research, read the appropriate section before selecting a response.

### Materials & experimental systems

n/a	Involved in the study
<input checked="" type="checkbox"/>	<input type="checkbox"/> Antibodies
<input checked="" type="checkbox"/>	<input type="checkbox"/> Eukaryotic cell lines
<input checked="" type="checkbox"/>	<input type="checkbox"/> Palaeontology and archaeology
<input type="checkbox"/>	<input checked="" type="checkbox"/> Animals and other organisms
<input checked="" type="checkbox"/>	<input type="checkbox"/> Clinical data
<input checked="" type="checkbox"/>	<input type="checkbox"/> Dual use research of concern
<input checked="" type="checkbox"/>	<input type="checkbox"/> Plants

### Methods

n/a	Involved in the study
<input checked="" type="checkbox"/>	<input type="checkbox"/> ChIP-seq
<input checked="" type="checkbox"/>	<input type="checkbox"/> Flow cytometry
<input checked="" type="checkbox"/>	<input type="checkbox"/> MRI-based neuroimaging

## Animals and other research organisms

Policy information about [studies involving animals](#); [ARRIVE guidelines](#) recommended for reporting animal research, and [Sex and Gender in Research](#)

#### Laboratory animals

NA

#### Wild animals

NA

#### Reporting on sex

NA

#### Field-collected samples

Tissue samples of fishes used in this study were loaned from research museum collections listed in the Acknowledgments and Table S1. Contact collection managers for information about long-term storage specific to each collection's policy.

## Ethics oversight

This study did not require IACUC approval because no live animals were used.

Note that full information on the approval of the study protocol must also be provided in the manuscript.

## Plants

Seed stocks

NA

Novel plant genotypes

NA

Authentication

NA